FIG. 3. Clinical features of patients with Kabuki syndrome harboring a MLL2 truncating-type mutation. A: Facial features of patients with Kabuki syndrome with a *MLL2* truncating-type mutation. The seven panels for patient KMS-54 show serial images at 0, 1, 4, 6.5, 9.5, 22, and 33 years of age, respectively. B: Complete right cleft lip/palate and lower lip pits (arrows) in patient KMS-41. C: Abnormal dentition in patients KMS-52 and KMS-59. They also showed hypodontia with wide interdentium. D: Patient KMS-72 had congenital strabismus and blepharoptosis as well as opacification of the cornea due to Peters anomaly (arrow). E: Hand images show short fifth fingers and prominent digit pads (white arrows).

FIG. 4. Clinical features of patients with Kabuki syndrome with a *MLL2* non-truncating-type mutation. A: Facial features of patients with KS and a *MLL2* non-truncating-type mutation. B: Patient KMS-56 showed abnormal dentition (hypodontia with wide interdentium).

Kokitsu-Nakata et al., 2012; Tanaka et al., 2012; Bogershausen and Wollnik, 2013; Makrythanasis et al., 2013] (Human Gene Mutation Database Professional 2012.3; https://portal.biobase-international.com/hgmd/pro/gene.php). Our mutation-positivity rate for either gene was 67.9% (55/81), and that for *MLL2* only was 61.7% (50/81); these figures are compatible with those reported in a review (55–80%) [Banka et al., 2012b]. Mutation-negative patients suggest the existence of unknown genes to cause KS or misdiagnosis.

As for the phenotype–genotype relationship, Banka et al. [2012b] suggested that feeding problems, kidney anomalies, premature thelarche, joint dislocation, and palatal malformation were more frequently observed in patients with *MLL2*-mutations than in patients with normal *MLL2* sequence. Hannibal et al. [2011] reported that renal anomalies were more common in patients who had *MLL2* mutations compared to those who did not. Li et al. [2011] reported that short stature and renal anomalies were more frequent in patients with *MLL2*-mutations than in those with normal *MLL2* sequence. In our study, premature thelarche was observed only in patients with *MLL2* mutations, but this was not significant ($P = 0.1137$). The frequencies of kidney anomalies, hip joint dislocation, and short stature were not different when comparing those with and without *MLL2* mutations ($P = 0.3030$, $P = 1.0000$, and $P = 0.0717$, respectively; Supplemental Table V). High arched eyebrows, palatal malformation (cleft palate/lip), low posterior hairline, and short fifth finger were more frequently observed in individuals with *MLL2* mutations than in patients with normal *MLL2* ($P = 0.0118$, $P = 0.0284$, $P = 0.0493$, and $P = 0.0137$, respectively; Supplemental Table V).

X-inactivation skewing in patients with KS has been discussed since the discovery of the *KDM6A* deletion in a female with KS

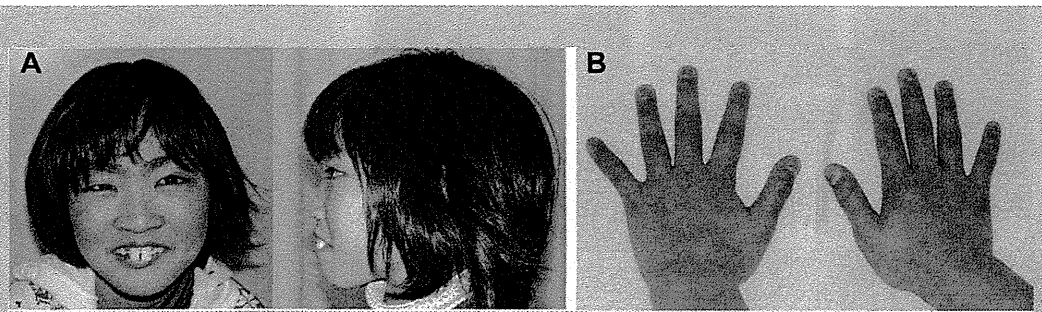

FIG. 5. Clinical features of patients with Kabuki syndrome with a *KDM6A* truncating-type mutation. A: Facial features of patient KMS-81 harboring a *KDM6A* mutation (c.1909_1912del, p.Ser637Thrfs*53). She showed large front teeth with wide interdentium. B: Hand image of KMS-81. Short fifth finger was not remarkable.

[Lederer et al., 2012; Miyake et al., 2013]. In two female patients reported here, patient KMS-65, who had an in-frame deletion, showed a random X-inactivation pattern, but patient KMS-81, who had a truncating-type mutation, showed marked skewing. X-inactivation skewing was also reported in two affected females with *KDM6A* deletion reported by Lederer et al. [2012]. cDNA sequence analysis of patient KMS-81 indicated that the mutant allele of *KDM6A* was expressed at a similar level to the wild-type allele under NMD inhibition. This result suggests that *KDM6A* mostly escapes X-inactivation in female lymphoblastoid cells. Interestingly, *KDM6A*/*Kdm6a* escapes X-inactivation in humans and mice, and in mice its expression level from the inactive X chromosome (Xi) was reported as 15–35% of that from the active X chromosome (Xa) [Greenfield et al., 1998; Xu et al., 2008]. We calculated the hypothetical expression assuming a 30% *KDM6A* expression level from Xi and 100% expression from Xa (Supplemental Fig. 2). In patient KMS-81, who showed marked skewing (98:2), either the mutant X chromosome or the wild-type X was inactivated in 98% of cells. If the mutant were inactivated, the expression level would be below 1 ($1.0 \times 0.98 + 0.3 \times 0.02 = 0.986$). If the wild-type were inactivated, the expression level would also be below 1 ($1.0 \times 0.02 + 0.3 \times 0.98 = 0.314$). The KS phenotype is usually unassociated with Turner syndrome (45,X), with the *KDM6A* expression level at 1.0 [Miyake et al., 2013]. It is possible that having a *KDM6A* expression level of 1.0 is essential for a normal human phenotype. Similarly, males with only one copy of *KDM6A* do not manifest KS. We previously mentioned the possibility of *UTY* compensation for *KMD6A* (Supplemental Fig. 2) [Miyake et al., 2013], although human UTY lacks demethylase activity [Hong et al., 2007; Lan et al., 2007]. The recent evidence that $X^{Utx-}X^{Utx-}$ homozygous mice demonstrated a more severe phenotype than $X^{Utx-}Y^{Uty+}$ mice indicates that UTY can compensate for the loss of UTX in embryonic development [Shpargel et al., 2012]. Because mouse and human UTY show 75% identity, and 95% identity in the Jumonji C domain [Shpargel et al., 2012], it is likely that normal human males who have only one copy of *KDM6A* are supplemented by *UTY* in a demethylase-independent manner.

Interestingly, $X^{Utx-}Y^{Uty+}$ mice showed small body size [Shpargel et al., 2012]. Similarly, the human *KDM6A*-mutated group exhibited short stature and postnatal growth retardation.

Regarding our mutation detection methods, HRM analysis and Sanger sequencing are both imperfect. Next-generation sequencing is more sensitive (especially for single nucleotide variants and small insertions/deletions), faster, and cheaper due to multiple gene screening and the potential to multiplex. However, a microdeletion involving *MLL2* or *KDM6A* or low-level mosaicism of a single nucleotide variant might be missed by this method. Therefore, in patients who test mutation-negative, more comprehensive approaches might be necessary. In conclusion, we investigated *MLL2* and *KDM6A* mutations and their clinical consequences in patients with KS. The majority of the clinical features were observed at a similar frequency among patients with either *MLL2* or *KDM6A*-mutations. The genetic basis of the patients who tested mutation-negative (20–45%) remains elusive. Further studies are necessary to understand the whole picture of the genetic aspects of KS and its genotype–phenotype relationships.

ACKNOWLEDGMENTS

We thank the patients and their parents for participating in this work. We also thank Ms. Y. Yamashita, Ms. E. Koike, Ms. S. Sugimoto, Ms. N. Watanabe, Ms. K. Takabe, and Mr. T. Miyama for their technical assistance. This work was supported by research grants from the Ministry of Health, Labour and Welfare of Japan (H. Saitsu, N. Matsumoto, N. Miyake), the Japan Science and Technology Agency (N. Matsumoto), the Strategic Research Program for Brain Sciences (N. Matsumoto), a Grant-in-Aid for Scientific Research on Innovative Areas-(Transcription cycle)-from the Ministry of Education, Culture, Sports, Science and Technology of Japan (N. Matsumoto), a Grant-in-Aid for Scientific Research from the Japan Society for the Promotion of Science (N. Matsumoto), a Grant-in-Aid for Young Scientists from the Japan Society for the Promotion of Science (H.S., N. Miyake), the Takeda Science Foundation (N. Matsumoto, N. Miyake), the Yokohama Foundation for the Advancement of Medical Science (N. Miyake), and the Hayashi Memorial Foundation for Female Natural Scientists (N. Miyake).

REFERENCES

Adzhubei IA, Schmidt S, Peshkin L, Ramensky VE, Gerasimova A, Bork P, Kondrashov AS, Sunyaev SR. 2010. A method and server for predicting damaging missense mutations. Nat Methods 7:248–249.

Allen RC, Zoghbi HY, Moseley AB, Rosenblatt HM, Belmont JW. 1992. Methylation of *Hpa*II and *Hha*I sites near the polymorphic CAG repeat in the human androgen-receptor gene correlates with X chromosome inactivation. Am J Hum Genet 51:1229–1239.

Banka S, Howard E, Bunstone S, Chandler K, Kerr B, Lachlan K, McKee S, Mehta S, Tavares A, Tolmie J, Donnai D. 2012a. MLL2 mosaic mutations and intragenic deletion-duplications in patients with Kabuki syndrome. Clin Genet 83:467–471.

Banka S, Veeramachaneni R, Reardon W, Howard E, Bunstone S, Ragge N, Parker MJ, Crow YJ, Kerr B, Kingston H, Metcalfe K, Chandler K, Magee A, Stewart F, McConnell VP, Donnelly DE, Berland S, Houge G, Morton JE, Oley C, Revencu N, Park SM, Davies SJ, Fry AE, Lynch SA, Gill H, Schweiger S, Lam WW, Tolmie J, Mohammed SN, Hobson E, Smith A, Blyth M, Bennett C, Vasudevan PC, Garcia-Minaur S, Henderson A, Goodship J, Wright MJ, Fisher R, Gibbons R, Price SM, CdS D, Temple IK, Collins AL, Lachlan K, Elmslie F, McEntagart M, Castle B, Clayton-Smith J, Black GC, Donnai D. 2012b. How genetically heterogeneous is Kabuki syndrome?: MLL2 testing in 116 patients, review and analyses of mutation and phenotypic spectrum. Eur J Hum Genet 20:381–388.

Bogershausen N, Wollnik B. 2013. Unmasking Kabuki syndrome. Clin Genet 83:201–211.

Dubuc AM, Remke M, Korshunov A, Northcott PA, Zhan SH, Mendez-Lago M, Kool M, Jones DT, Unterberger A, Morrissy AS, Shih D, Peacock J, Ramaswamy V, Rolider A, Wang X, Witt H, Hielscher T, Hawkins C, Vibhakar R, Croul S, Rutka JT, Weiss WA, Jones SJ, Eberhart CG, Marra MA, Pfister SM, Taylor MD. 2013. Aberrant patterns of H3K4 and H3K27 histone lysine methylation occur across subgroups in medulloblastoma. Acta Neuropathol 125:373–384.

Greenfield A, Carrel L, Pennisi D, Philippe C, Quaderi N, Siggers P, Steiner K, Tam PP, Monaco AP, Willard HF, Koopman P. 1998. The UTX gene escapes X inactivation in mice and humans. Hum Mol Genet 7:737–742.

Hannibal MC, Buckingham KJ, Ng SB, Ming JE, Beck AE, McMillin MJ, Gildersleeve HI, Bigham AW, Tabor HK, Mefford HC, Cook J, Yoshiura K, Matsumoto T, Matsumoto N, Miyake N, Tonoki H, Naritomi K,

Kaname T, Nagai T, Ohashi H, Kurosawa K, Hou JW, Ohta T, Liang D, Sudo A, Morris CA, Banka S, Black GC, Clayton-Smith J, Nickerson DA, Zackai EH, Shaikh TH, Donnai D, Niikawa N, Shendure J, Bamshad MJ. 2011. Spectrum of MLL2 (ALR) mutations in 110 cases of Kabuki syndrome. Am J Med Genet Part A 155A:1511–1516.

Hong S, Cho YW, Yu LR, Yu H, Veenstra TD, Ge K. 2007. Identification of JmjC domain-containing UTX and JMJD3 as histone H3 lysine 27 demethylases. Proc Natl Acad Sci USA 104:18439–18444.

Ito N, Ihara K, Tsutsumi Y, Miyake N, Matsumoto N, Hara T. 2013. Hypothalamic pituitary complications in Kabuki syndrome. Pituitary 16:133–138.

Kokitsu-Nakata NM, Petrin AL, Heard JP, Vendramini-Pittoli S, Henkle LE, dos Santos DV, Murray JC, Richieri-Costa A. 2012. Analysis of MLL2 gene in the first Brazilian family with Kabuki syndrome. Am J Med Genet Part A 158A:2003–2008.

Kuroki Y, Suzuki Y, Chyo H, Hata A, Matsui I. 1981. A new malformation syndrome of long palpebral fissures, large ears, depressed nasal tip, and skeletal anomalies associated with postnatal dwarfism and mental retardation. J Pediatr 99:570–573.

Lan F, Bayliss PE, Rinn JL, Whetstine JR, Wang JK, Chen S, Iwase S, Alpatov R, Issaeva I, Canaani E, Roberts TM, Chang HY, Shi Y. 2007. A histone H3 lysine 27 demethylase regulates animal posterior development. Nature 449:689–694.

Lederer D, Grisart B, Digilio MC, Benoit V, Crespin M, Ghariani SC, Maystadt I, Dallapiccola B, Verellen-Dumoulin C. 2012. Deletion of KDM6A, a histone demethylase interacting with MLL2, in three patients with Kabuki syndrome. Am J Hum Genet 90:119–124.

Lee MG, Villa R, Trojer P, Norman J, Yan KP, Reinberg D, Di Croce L, Shiekhattar R. 2007. Demethylation of H3K27 regulates polycomb recruitment and H2A ubiquitination. Science 318:447–450.

Li Y, Bogershausen N, Alanay Y, Simsek Kiper PO, Plume N, Keupp K, Pohl E, Pawlik B, Rachwalski M, Milz E, Thoenes M, Albrecht B, Prott EC, Lehmkuhler M, Demuth S, Utine GE, Boduroglu K, Frankenbusch K, Borck G, Gillessen-Kaesbach G, Yigit G, Wieczorek D, Wollnik B. 2011. A mutation screen in patients with Kabuki syndrome. Hum Genet 130:715–724.

Makrythanasis P, van Bon BW, Steehouwer M, Rodriguez-Santiago B, Simpson M, Dias P, Anderlid BM, Arts P, Bhat M, Augello B, Biamino E, Bongers EM, Del Campo M, Cordeiro I, Cueto-Gonzalez AM, Cusco I, Deshpande C, Frysira E, Louise I, Flores R, Galan E, Gener B, Gilissen C, Granneman SM, Hoyer J, Yntema HG, Kets CM, Koolen DA, Marcelis CL, Medeira A, Micale L, Mohammed S, de Munnik SA, Nordgren A, Reardon SP, Revencu N, Roscioli T, Ruiterkamp-Versteeg M, Santos HG, Schoumans J, Schuurs-Hoeijmakers JH, Silengo MC, Toledo L, Vendrell T, van der Burgt I, van Lier B, Zweier C, Reymond A, Trembath RC, Perez-Jurado L, Dupont J, de Vries BB, Brunner HG, Veltman JA, Merla G, Antonarakis SE, Hoischen A. 2013. MLL2 mutation detection in 86 patients with Kabuki syndrome: A genotype–phenotype study. Clin Genet (In Press).

Micale L, Augello B, Fusco C, Selicorni A, Loviglio MN, Silengo MC, Reymond A, Gumiero B, Zucchetti F, D'Addetta EV, Belligni E, Calcagni A, Digilio MC, Dallapiccola B, Faravelli F, Forzano F, Accadia M, Bonfante A, Clementi M, Daolio C, Douzgou S, Ferrari P, Fischetto R, Garavelli L, Lapi E, Mattina T, Melis D, Patricelli MG, Priolo M, Prontera P, Renieri A, Mencarelli MA, Scarano G, della Monica M, Toschi B, Turolla L, Vancini L, Zatterale A, Gabrielli O, Zelante L, Merla G. 2011. Mutation spectrum of MLL2 in a cohort of Kabuki syndrome patients. Orphanet J Rare Dis 6:38.

Miyake N, Mizuno S, Okamoto N, Ohashi H, Shiina M, Ogata K, Tsurusaki Y, Nakashima M, Saitsu H, Niikawa N, Matsumoto N. 2013. KDM6A point mutations cause Kabuki syndrome. Hum Mutat 34:108–110.

Ng SB, Bigham AW, Buckingham KJ, Hannibal MC, McMillin MJ, Gildersleeve HI, Beck AE, Tabor HK, Cooper GM, Mefford HC, Lee C, Turner EH, Smith JD, Rieder MJ, Yoshiura K, Matsumoto N, Ohta T, Niikawa N, Nickerson DA, Bamshad MJ, Shendure J. 2010. Exome sequencing identifies MLL2 mutations as a cause of Kabuki syndrome. Nat Genet 42:790–793.

Niikawa N, Matsuura N, Fukushima Y, Ohsawa T, Kajii T. 1981. Kabuki make-up syndrome: A syndrome of mental retardation, unusual facies, large and protruding ears, and postnatal growth deficiency. J Pediatr 99:565–569.

Niikawa N, Kuroki Y, Kajii T, Matsuura N, Ishikiriyama S, Tonoki H, Ishikawa N, Yamada Y, Fujita M, Umemoto H, Iwama Y, Kondoh I, Fukushima Y, Nako Y, Matsui I, Urakami T, Aritaki S, Hara M, Suzuki Y, Chyo H, Sugio Y, Hasegawa T, Yamanaka T, Tsukino R, Yoshida A, Nomoto N, Kawahito S, Aihara R, Toyota S, Ieshima A, Funaki H, Ishitobi K, Ogura S, Furumae T, Yoshino M, Tsuji Y, Kondoh T, Matsumoto T, Abe K, Harada N, Miike T, Ohdo S, Naritomi K, Abushwereb AK, Braun OH, Schmid E. 1988. Kabuki make-up (Niikawa–Kuroki) syndrome: A study of 62 patients. Am J Med Genet 31:565–589.

Paulussen AD, Stegmann AP, Blok MJ, Tserpelis D, Posma-Velter C, Detisch Y, Smeets EE, Wagemans A, Schrander JJ, van den Boogaard MJ, van der Smagt J, van Haeringen A, Stolte-Dijkstra I, Kerstjens-Frederikse WS, Mancini GM, Wessels MW, Hennekam RC, Vreeburg M, Geraedts J, de Ravel T, Fryns JP, Smeets HJ, Devriendt K, Schrander-Stumpel CT. 2011. MLL2 mutation spectrum in 45 patients with Kabuki syndrome. Hum Mutat 32:E2018–E2025.

Prasad R, Zhadanov AB, Sedkov Y, Bullrich F, Druck T, Rallapalli R, Yano T, Alder H, Croce CM, Huebner K, Mazo A, Canaani E. 1997. Structure and expression pattern of human ALR, a novel gene with strong homology to ALL-1 involved in acute leukemia and to Drosophila trithorax. Oncogene 15:549–560.

Schuettengruber B, Chourrout D, Vervoort M, Leblanc B, Cavalli G. 2007. Genome regulation by polycomb and trithorax proteins. Cell 128:735–745.

Schwarz JM, Rodelsperger C, Schuelke M, Seelow D. 2010. MutationTaster evaluates disease-causing potential of sequence alterations. Nat Methods 7:575–576.

Shpargel KB, Sengoku T, Yokoyama S, Magnuson T. 2012. UTX and UTY demonstrate histone demethylase-independent function in mouse embryonic development. PLoS Genet 8:e1002964.

Tanaka R, Takenouchi T, Uchida K, Sato T, Fukushima H, Yoshihashi H, Takahashi T, Tsubota K, Kosaki K. 2012. Congenital corneal staphyloma as a complication of Kabuki syndrome. Am J Med Genet Part A 158A:2000–2002.

Tekin M, Fitoz S, Arici S, Cetinkaya E, Incesulu A. 2006. Niikawa–Kuroki (Kabuki) syndrome with congenital sensorineural deafness: Evidence for a wide spectrum of inner ear abnormalities. Int J Pediatr Otorhinolaryngol 70:885–889.

Torii Y, Yagasaki H, Tanaka H, Mizuno S, Nishio N, Muramatsu H, Hama A, Takahashi Y, Kojima S. 2009. Successful treatment with rituximab of refractory idiopathic thrombocytopenic purpura in a patient with Kabuki syndrome. Int J Hematol 90:174–176.

Tsurusaki Y, Kobayashi Y, Hisano M, Ito S, Doi H, Nakashima M, Saitsu H, Matsumoto N, Miyake N. 2013. The diagnostic utility of exome sequencing in Joubert syndrome and related disorders. J Hum Genet 58:113–115.

Xu J, Deng X, Watkins R, Disteche CM. 2008. Sex-specific differences in expression of histone demethylases Utx and Uty in mouse brain and neurons. J Neurosci 28:4521–4527.

ARTICLE

De Novo Mutations in *GNAO1*, Encoding a $G\alpha_o$ Subunit of Heterotrimeric G Proteins, Cause Epileptic Encephalopathy

Kazuyuki Nakamura,[1,2,9] Hirofumi Kodera,[1,9] Tenpei Akita,[3,9] Masaaki Shiina,[4] Mitsuhiro Kato,[2] Hideki Hoshino,[5] Hiroshi Terashima,[5] Hitoshi Osaka,[6] Shinichi Nakamura,[7] Jun Tohyama,[8] Tatsuro Kumada,[3] Tomonori Furukawa,[3] Satomi Iwata,[3] Takashi Shiihara,[2,10] Masaya Kubota,[5] Satoko Miyatake,[1] Eriko Koshimizu,[1] Kiyomi Nishiyama,[1] Mitsuko Nakashima,[1] Yoshinori Tsurusaki,[1] Noriko Miyake,[1] Kiyoshi Hayasaka,[2] Kazuhiro Ogata,[4] Atsuo Fukuda,[3] Naomichi Matsumoto,[1,*] and Hirotomo Saitsu[1,*]

Heterotrimeric G proteins, composed of α, β, and γ subunits, can transduce a variety of signals from seven-transmembrane-type receptors to intracellular effectors. By whole-exome sequencing and subsequent mutation screening, we identified de novo heterozygous mutations in *GNAO1*, which encodes a $G\alpha_o$ subunit of heterotrimeric G proteins, in four individuals with epileptic encephalopathy. Two of the affected individuals also showed involuntary movements. Somatic mosaicism (approximately 35% to 50% of cells, distributed across multiple cell types, harbored the mutation) was shown in one individual. By mapping the mutation onto three-dimensional models of the Gα subunit in three different complexed states, we found that the three mutants (c.521A>G [p.Asp174Gly], c.836T>A [p.Ile279Asn], and c.572_592del [p.Thr191_Phe197del]) are predicted to destabilize the Gα subunit fold. A fourth mutant (c.607G>A), in which the Gly203 residue located within the highly conserved switch II region is substituted to Arg, is predicted to impair GTP binding and/or activation of downstream effectors, although the p.Gly203Arg substitution might not interfere with Gα binding to G-protein-coupled receptors. Transient-expression experiments suggested that localization to the plasma membrane was variably impaired in the three putatively destabilized mutants. Electrophysiological analysis showed that $G\alpha_o$-mediated inhibition of calcium currents by norepinephrine tended to be lower in three of the four $G\alpha_o$ mutants. These data suggest that aberrant $G\alpha_o$ signaling can cause multiple neurodevelopmental phenotypes, including epileptic encephalopathy and involuntary movements.

Introduction

Epileptic encephalopathy is a group of neurological disorders characterized by severe and progressive cognitive and behavioral impairments, which are most likely caused or made worse by epileptic activity.[1] Ohtahara syndrome (OS [MIM 308350 and 612164]) is the most severe and the earliest form of epileptic encephalopathy and is characterized by tonic spasms mainly in the neonatal period, seizure intractability, and a suppression-burst pattern on electroencephalography (EEG).[2] De novo mutations in three genes, *ARX* (MIM 300382), *STXBP1* (MIM 602926), and *KCNQ2* (MIM 602235), have been reported in individuals with OS.[3–6]

Heterotrimeric guanine-binding proteins (G proteins) are composed of α, β, and γ subunits. In its basal state, Gα is bound with guanosine diphosphate (GDP) and forms the Gαβγ complex. When a seven-transmembrane-type receptor binds its agonist, it activates G proteins by catalyzing the exchange of GDP for guanosine triphosphate (GTP) on the Gα subunit. Subsequently, GTP-bound Gα dissociates from Gβγ, and each of the two complexes activates distinct downstream effectors.[7] In mammals, Gα subunits are divided into four classes: $G\alpha_{i/o}$, $G\alpha_{q/11}$, $G\alpha_s$, and $G\alpha_{12/13}$.[7] $G\alpha_o$, encoded by *GNAO1* (MIM 139311), is extremely abundant in brain tissue, where it can constitute up to approximately 0.5% of membrane protein,[8] suggesting important roles in brain function. In fact, mice lacking $G\alpha_o$ show multiple neurological abnormalities, including generalized tremor, occasional seizures, severe motor-control impairment, hyperalgesia, and behavioral abnormalities with early postnatal lethality.[9,10]

In this study, de novo *GNAO1* mutations were identified in four epileptic-encephalopathy-affected individuals, three of whom were diagnosed with OS. In addition, two of the four individuals showed involuntary movements, suggesting that aberration of $G\alpha_o$ can cause multiple neurodevelopmental phenotypes.

[1]Department of Human Genetics, Yokohama City University Graduate School of Medicine, 3-9 Fukuura, Kanazawa-ku, Yokohama 236-0004, Japan; [2]Department of Pediatrics, Yamagata University Faculty of Medicine, 2-2-2 Iida-nishi, Yamagata 990-9585, Japan; [3]Department of Neurophysiology, Hamamatsu University School of Medicine, 1-20-1 Handayama, Higashi-ku, Hamamatsu 431-3192, Japan; [4]Department of Biochemistry, Yokohama City University Graduate School of Medicine, 3-9 Fukuura, Kanazawa-ku, Yokohama 236-0004, Japan; [5]Division of Neurology, National Center for Child Health and Development, 2-10-1 Okura, Setagaya-ku, Tokyo 157-8535, Japan; [6]Division of Neurology, Clinical Research Institute, Kanagawa Children's Medical Center, 2-138-4 Mutsukawa, Minami-ku, Yokohama 232-8555, Japan; [7]Department of Pediatrics, Nagano Red Cross Hospital, 5-22-1 Wakasato, Nagano 380-8582, Japan; [8]Department of Pediatrics, Epilepsy Center, Nishi-Niigata Chuo National Hospital, Niigata 950-2085, Japan
[9]These authors contributed equally to this work
[10]Present address: Department of Neurology, Gunma Children's Medical Center, 779 Shimohakoda Hokkitsu-machi, Shibukawa, Gunma 377-8577, Japan
*Correspondence: naomat@yokohama-cu.ac.jp (N.M.), hsaitsu@yokohama-cu.ac.jp (H.S.)
http://dx.doi.org/10.1016/j.ajhg.2013.07.014.

Subjects and Methods

Subjects

Twelve individuals with OS were previously analyzed by whole-exome sequencing (WES).[3,11] In addition, we analyzed parental samples from 5 of the 12 individuals by WES. Screening for *GNAO1* mutations was performed in 367 individuals with epileptic encephalopathy (including 62 OS cases) by high-resolution-melting (HRM) analysis (339 cases) and/or WES (100 cases). The diagnosis was made on the basis of clinical features and characteristic patterns on EEG. Experimental protocols were approved by the institutional review board of Yokohama City University School of Medicine and Yamagata University Faculty of Medicine. Informed consent was obtained from the families of all individuals.

DNA Samples

Genomic DNA was obtained from peripheral-blood leukocytes by standard methods. For detection of a mosaic mutation in individual 2, genomic DNA from saliva and nails was isolated with an Oragene DNA kit (DNA Genotek) and an ISOHAIR kit (Nippon Gene), respectively.

WES

Genomic DNA was captured with the SureSelect Human All Exon v.4 Kit (Agilent Technologies) and sequenced with four samples per lane on an Illumina HiSeq 2000 (Illumina) with 101 bp paired-end reads. Image analysis and base calling were performed by Sequencing Control Software with Real-Time Analysis and CASAVA software v.1.8 (Illumina). Exome data processing, variant calling, and variant annotation were performed as previously described.[12–14] Reads were aligned to GRCh37 with Novoalign (Novocraft Technologies). Duplicate reads were removed with Picard, and local realignments around indels and base-quality-score recalibration were performed with the Genome Analysis Toolkit (GATK).[13] Single-nucleotide variants and small indels were identified with the GATK UnifiedGenotyper and were filtered according to the Broad Institute's best-practice guidelines v.3. Not flagged as clinically associated, variants registered in dbSNP135 were filtered. Filter-passed variants were annotated with ANNOVAR.[14] Pathogenic mutations detected by WES were confirmed by Sanger sequencing.

Mutation Screening

Genomic DNA was amplified with an illustra GenomiPhi V2 DNA Amplification Kit (GE Healthcare). Exons 1–8 covering the *GNAO1* coding region of two transcript variants (transcript variant 1, RefSeq accession number NM_020988.2, encoding $G\alpha_{o1}$; transcript variant 2, RefSeq accession number NM_138736.2, encoding $G\alpha_{o2}$) were screened by HRM analysis. The last two exons differ between the transcript variants. HRM analysis was performed with a Light Cycler 480 (Roche Diagnostics). Samples showing an aberrant melting curve in the HRM analysis were sequenced. PCR primers and conditions are shown in Table S1, available online. All mutations not present in publically available databases were verified with original genomic DNA and were searched for in the variant database of our 408 in-house control exomes.

Deep Sequencing of a Mosaic Mutation

PCR products (length 178 bp) spanning the c.521A>G mutation were amplified with the use of blood, saliva, and nail DNA samples from individual 2 and blood DNA samples from her parents as a template. Adaptor ligation, nick repair, and amplification were performed with the Ion Xpress Plus Fragment Library Kit (Life Technologies) according to the manufacturer's protocol (part no. 4471989 Rev. B). Indexing was carried out with the Xpress Barcode Adapters 1–16 Kit (Life Technologies). Emulsion PCR and enrichment steps were carried out with the Ion OneTouch 200 Template Kit v.2 (Life Technologies) according to the manufacturer's protocol (part no. 4478371 Rev. A). Sequencing of the amplicon libraries was carried out on the Ion Torrent Personal Genome Machine (PGM) with the Ion 314 sequencing chip and the Ion PGM 200 Sequencing Kit (Life Technologies) according to the recommended protocol (part no. 4474246 Rev. B). Torrent Suite 2.2 was used for all analyses. The percentage of mosaicism was examined with the Integrative Genomics Viewer.[15,16]

Expression Vectors

A full-length human *GNAO1* cDNA clone (transcript variant 1, encoding $G\alpha_{o1}$) was purchased from Kazusa DNA Research Institute. Human *GNAO1* cDNA was inserted into a pEF6/V5-His-C vector for the introduction of a C-terminal V5 epitope (Life Technologies). Site-directed mutagenesis using a KOD-Plus-Mutagenesis kit (Toyobo) was performed for generating *GNAO1* mutants, including c.521A>G (p.Asp174Gly), c.572_592del (p.The191_Phe197del), c.836T>A (p.Ile279Asn), and c.607G>A (p.Gly203Arg). A c.607_609delinsACA (p.Gly203Thr) mutant, in which GTP binding was reversible in contrast to the WT,[17] was also generated to serve as the known loss-of-function mutant.[18] All variant cDNAs were confirmed by Sanger sequencing.

Immunofluorescence Microscopy

Mouse neuroblastoma 2A (N2A) cells were grown as previously described.[4] N2A cells on glass coverslips were transfected with 200 ng of plasmid DNA with the use of X-tremeGENE 9 DNA Transfection Reagent (Roche Diagnostics). After 24 hr, cells were fixed in PBS containing 4% paraformaldehyde for 15 min and permeabilized in PBS containing 0.1% Triton X-100 for 5 min. Cells were then blocked with 10% normal goat serum for 30 min. V5-tagged $G\alpha_{o1}$ was detected with a mouse V5 antibody (1:200 dilution; Life Technologies) and Alexa-488-conjugated goat anti-mouse IgG (1:1000 dilution; Life Technologies). Coverslips were mounted with Vectashield (Vector Laboratories) that contained DAPI and were visualized with an inverted FV1000-D confocal microscope (Olympus).

Structural Modeling and Free-Energy Calculations

We used FoldX software (version 3.0β5) to construct mutated molecular structures and calculate the free-energy changes caused by the mutations.[19] We used crystal structures of the GDP-bound inactive $G\alpha_i\beta\gamma$ heterotrimer (Protein Data Bank [PDB] 1GG2),[20] the nucleotide-free $G\alpha_s\beta\gamma$ in complex with agonist-occupied monomeric β2 adrenergic receptor (β2AR) (PDB 3SN6),[21] and the transition-state analog of GTP ($GDP^+AlF_4^-$)-bound $G\alpha_q$ in complex with its effector phospholipase C-β (PLCβ) (PDB 3OHM)[22] as three-dimensional structure models of the $G\alpha_o$ subunit in different complexed states. Each of the mutations, corresponding to p.Asp174Gly, p.Ile279Asn, or p.Gly203Arg in the human $G\alpha_o$ subunit, was introduced into the Gα subunit of each complex, and the free-energy change upon the mutation was calculated with FoldX software. Note that ligands included in the complexes were ignored in the calculation because the FoldX energy function

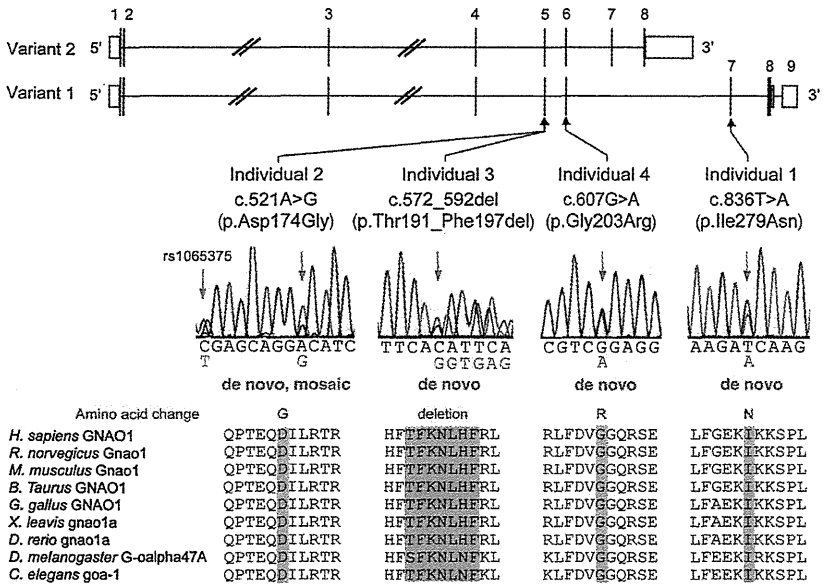

Figure 1. De Novo *GNAO1* Mutations in Individuals with Epileptic Encephalopathy
Schematic representation of *GNAO1*, including two transcript variants: transcript variant 1 (RefSeq NM_020988.2) with nine exons and transcript variant 2 (RefSeq NM_138736.2) with eight exons. The UTRs and coding regions are shown in white and black rectangles, respectively. Three mutations occurred in common exons of two transcript variants, and one mutation occurred uniquely in transcript variant 1. Note that the electropherogram of individual 2 suggested mosaicism of the c.521A>G mutation, and a heterozygous C>T change (rs1065375) was clearly demonstrated. All mutations caused substitution or deletion of evolutionarily conserved amino acids. Homologous sequences were aligned with the use of the CLUSTALW web site.

does not consider the contribution of ligands. The calculation was repeated three times, and the resultant data were presented as an average value with a SD.

Electrophysiology

For electrophysiological recording of calcium currents, we used NG108-15 cells transfected with individual *GNAO1* mutants. Expression vectors were introduced by electroporation with the Lonza Nucleofector device and the Cell Line Nucleofector Kit V (Lonza) according to the manufacture's protocol (program X-023). Two micrograms of plasmid DNA was used per transfection. The transfected cells were plated on poly-L-lysine-coated plastic coverslips (Cell Desk LF, MS-0113L; Sumitomo Bakelite) at a density of about 5×10^4 cells/cm^2 and cultured in Dulbecco's modified Eagle's medium (DMEM) supplemented with 10% fetal bovine serum (FBS). One day after transfection, the cells were differentiated with DMEM supplemented with 10 μM prostaglandin E1, 50 μM IBMX, and 1% FBS for 3–7 days before recording. During the culture period, half of the medium was changed every other day.

The recording was made by the perforated whole-cell patch-clamp technique with amphotericin B. Cells on coverslips were perfused under an Olympus BX51W upright microscope (Olympus) with a bath solution containing 140 mM NaCl, 5 mM $CaCl_2$, 4 mM KCl, 1 mM $MgCl_2$, 10 mM HEPES, 10 mM TEACl, 8 mM glucose, and 0.0002 mM tetrodotoxin (pH 7.3 adjusted with NaOH). The patch pipette solution contained 100 mM CsCl, 10 mM EGTA, and 40 mM HEPES (pH 7.3 adjusted with CsOH). Amphotericin B was added to the pipette solution at 2 μl/ml just before the experiments. The pipettes were fabricated from borosilicate glass capillaries and had a resistance of 4–8 MΩ when backfilled with the amphotericin-B-containing pipette solution. The recording was started when the series resistance was reduced to <150 MΩ after gigaseal formation and clear cellular capacitive surges had appeared. Voltage-gated calcium currents were elicited by the application of 50 ms depolarizing pulses to +10 mV from the holding potential of −65 mV, recorded with a Multiclamp 700B (Molecular Devices) controlled via pCLAMP10 software (Molecular Devices), filtered at 2 kHz, and sampled at 10 kHz with 50% compensation for series resistance. $G\alpha_o$-mediated current inhibition was elicited by the application of 10 μM norepinephrine via the bath solution. After 3–5 min, inhibition was assessed by measurement of the changes in current density just before the end of the depolarizing pulses. Recordings were made at room temperature.

Statistical multiple comparisons were made with ANOVA followed by Dunnett's post hoc test, and the threshold p value for judging statistical significance was 0.05. The current inhibition induced by norepinephrine in individual mutant-expressing cells was assessed with a paired t test. The results are given as the mean ± SEM.

Results

GNAO1 Is Mutated in Individuals with Epileptic Encephalopathy

We previously performed WES of 12 individuals with OS.[3,11] In this study, we analyzed parental samples from 5 of the 12 individuals by WES (mean RefSeq read depth of 109) to systematically screen de novo or recessive mutations. We found no recessive mutations in *SLC25A22* (MIM 609302), *PNPO* (MIM 610090), *PNKP* (MIM 613402), *PLCB1* (MIM 613722), or *ST3GAL3* (MIM 615006), whose mutations were previously found in epileptic encephalopathy,[23–27] but we did find one or two de novo mutations in each of the five trio exomes. Among them, a de novo missense mutation (c.836T>A [p.Ile279Asn]) in *GNAO1* at 16q12.2 was identified in individual 1. In the exome data of the other seven original individuals, we also found in individual 2 a second missense mutation (c.521A>G [p.Asp174Gly]), which was confirmed as a de novo event by Sanger sequencing (Figure 1). Moreover, *GNAO1* mutation screening in 367 individuals with epileptic encephalopathy by HRM analysis (339 individuals) and/or WES (100 individuals,

Table 1. Clinical Features of Individuals with a *GNAO1* Mutation

	Individual 1	Individual 2	Individual 3	Individual 4
Gender	female	female	female	female
Age	13 years	4 years, 1 month	died at 11 months	8 years
Mutation	c.836T>A (p.Ile279Asn)	c.521A>G (p.Asp174Gly)	c.572_592 del (p.Thr191_Phe197 del)	c.607G>A (p.Gly203Arg)
Inheritance	de novo	de novo, somatic mosaic	de novo	de novo
Diagnosis	Ohtahara syndrome	Ohtahara syndrome	Ohtahara syndrome	epileptic encephalopathy
Initial symptom	tonic seizure at 4 days	series of tonic seizures at 29 days (tonic upgaze, head nodding, extension of all extremities)	series of tonic seizures at 2 weeks (resemble spasms)	opisthotonic posture, developmental delay at 7 months
Initial EEG	suppression-burst pattern at 4 days	suppression-burst pattern at 29 days	suppression-burst pattern at 2 weeks	diffuse irregular spike-and-slow-wave complex at 5 years
Course of seizures	tonic seizure at 5 years	series of tonic seizures at 9 months	tonic seizure at 10 months	focal seizure (tonic upgaze), tonic seizure at 5 years
Course of EEG	multifocal sharp waves at 1 year, 4 months; suppression-burst pattern at 5 years, 6 months	hypsarrhythmia at 3 months; diffuse spike-and-slow-wave complex at 1 year, 7 months; sharp waves at frontal lobe at 3 years, 9 months	hypsarrhythmia at 4 months	not done
Involuntary movement	-	-	dystonia	severe chorea, athetosis
Seizure control	intractable (2–3 times per day)	intractable (0–2 times per day)	intractable	intractable (several times per day)
Development				
Head control	-	+	-	-
Sitting	-	-	-	-
Meaningful words	-	-	-	-
MRI	normal at 1 month; cerebral atrophy at 5 years, 6 months	delayed myelination and thin corpus callosum at 10 months	normal at 3 months	delayed myelination at 1 year, 3 months; reduced cerebral white matter, thin corpus callosum at 4 years, 8 months

mean read depth of 129) revealed two de novo mutations: c.572_592 del (p.Thr191_Phe197del) in individual 3 and c.607G>A (p.Gly203Arg) in individual 4 (Figure 1). One mutation (c.836T>A) specifically affects *GNAO1* transcript variant 1, whereas the other three mutations affect both transcript variants 1 and 2. Web-based prediction tools suggested that these four mutations would be pathogenic (Table S2). None of the four mutations was found in the 6,500 exomes of the National Heart, Lung, and Blood Institute (NHLBI) Exome Sequencing Project Exome Variant Server or among our 408 in-house control exomes. Interestingly, exome data and Sanger sequencing indicated that the c.521A>G mutation in individual 2 was somatic mosaic (Figure 1 and Table S3). We confirmed de novo somatic mosaicism of the c.521A>G mutation by deep sequencing of PCR products amplified with blood, nail, and saliva DNA from individual 2 and blood DNA from her parents, showing that approximately 35%–50% of cells harbored the mutation (Table S3).

Phenotypes Associated with *GNAO1* Mutations

Neurological features of four female individuals with *GNAO1* mutations are shown in Table 1. Three individuals (individuals 1–3) developed tonic seizures with suppression-burst pattern on EEG at the onset (range 4–29 days), leading to a diagnosis of OS. Individuals 2 and 3 transited to West syndrome, a common infantile epileptic syndrome, as revealed by hypsarrhythmia on EEG at 3–4 months of age (Figures 2A–2C). Individual 4 showed developmental delay and opisthotonic posture at 7 months of age, and complex partial seizures with epileptic discharge on EEG was observed at 5 years (Figure 2D). Of note, two individuals showed involuntary movements: individual 3 showed dystonia, and individual 4 displayed chorea and athetosis (Table 1 and Movie S1). Brain MRI showed delayed myelination in individuals 2 and 4, cerebral atrophy or reduced cerebral white matter in individuals 1 and 4, and thin corpus callosum in individuals 2 and 4 (Figures 2E–2I). Although seizures and EEG

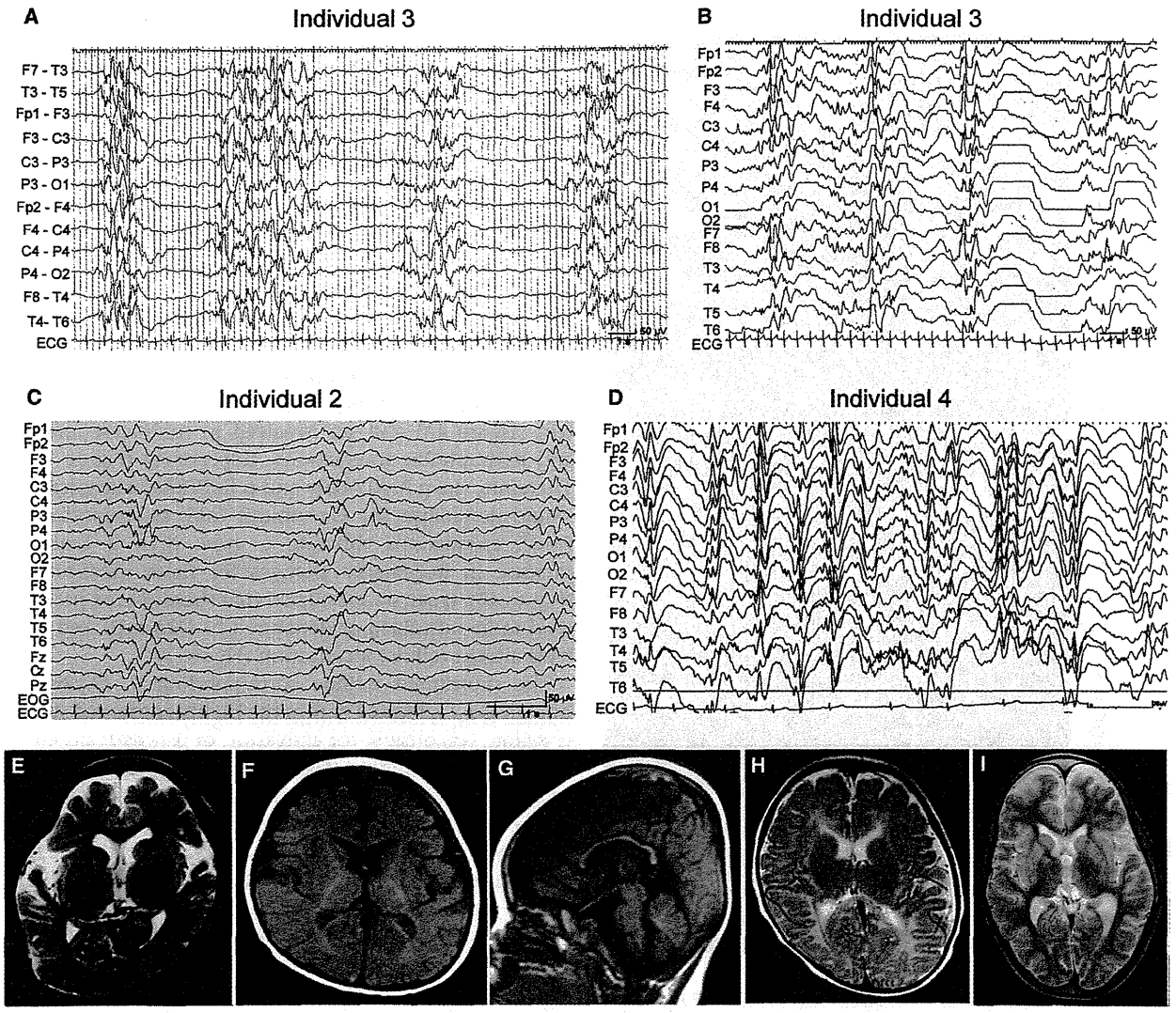

Figure 2. EEG and Brain MRI Features of Individuals with *GNAO1* Mutations
(A and B) Interictal EEG of individual 3. A suppression-burst pattern was observed at 2 months of age (A), and transition to hypsarrhythmia was observed at 4 months (B).
(C) Interictal EEG of individual 2 shows a suppression-burst pattern at 2 months.
(D) Interictal EEG of individual 4 shows a diffuse spike- or sharp-and-slow-wave complex at 5 years.
(E–I) T2-weighted axial images through the basal ganglia (E, H, and I) and T1-weighted axial (F) and sagittal (G) images. Individual 1 showed cerebral atrophy at 5 years and 6 months (E). Individual 2 showed delayed myelination and thin corpus callosum at 10 months (F and G). Individual 3 showed normal appearance at 3 months (H). Individual 4 showed reduced white matter at 7 years (I).

findings in two individuals with OS (individuals 2 and 3) were temporarily improved by adrenocorticotropic hormone therapy and valproic acid, all four individuals had intractable epileptic seizures in spite of combinatory therapy of antiepileptic drugs. All individuals had severe intellectual disability and motor developmental delay, and individual 3 died at 11 months because of respiratory-tract obstruction. These data suggest that *GNAO1* mutations can cause multiple neurodevelopmental phenotypes, including epileptic encephalopathy and involuntary movements.

Expression of Mutant $G\alpha_{o1}$ in N2A Cells

To examine the mutational effect of four *GNAO1* mutations, we performed transient expression experiments in N2A cells (Figure 3). C-terminally V5-epitope-tagged wild-type (WT) $G\alpha_{o1}$, encoded by transcript variant 1, was clearly localized in the cell periphery, as previously reported.[28] The p.Gly203Thr (with known loss of function)[17] and p.Gly203Arg (in individual 4) altered proteins were also localized in the cell periphery. In contrast, the p.Thr191_Phe197del altered protein (in individual 3) accumulated in the cytosolic compartment. The p.Asp174Gly

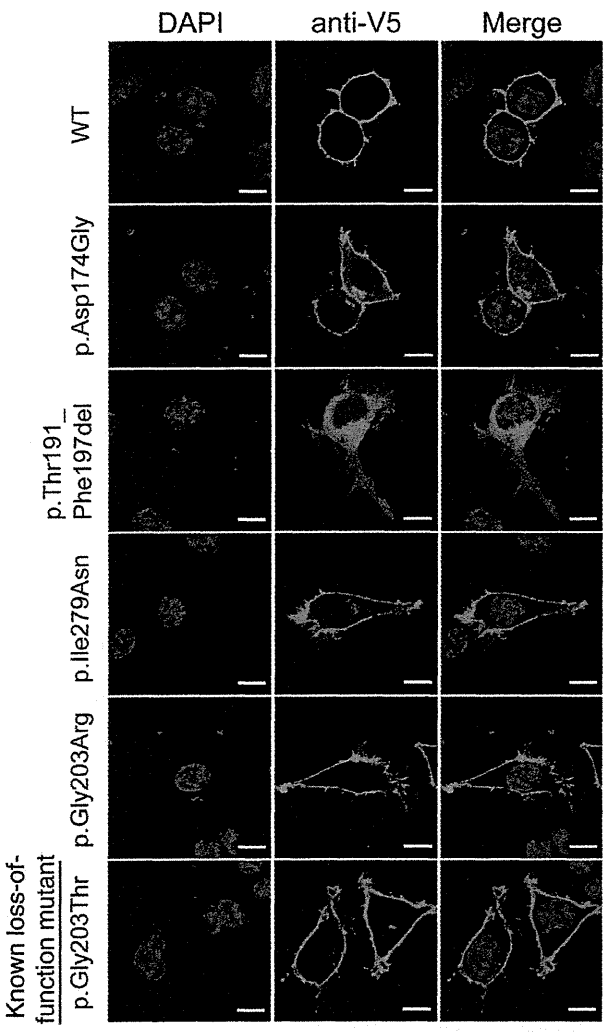

Figure 3. Localization of V5-Tagged $G\alpha_{o1}$ Proteins in N2A Cells
Localization of WT and five altered $G\alpha_{o1}$ proteins in N2A cells. The WT and p.Gly203Arg and p.Gly203Thr altered proteins were localized to the cell periphery. In contrast, the p.Thr191_Phe197del protein was localized to the cytosolic compartment. The other p.Asp174Gly and p.Ile279Asn proteins were localized to the cell periphery but were also observed in the cytosol. The scale bars represent 10 μm.

(individual 2) and p.Ile279Asn (individual 1) altered proteins were localized to the cell periphery and had weak signal in the cytosol, where more intense signal was observed in the p.Asp174Gly protein. Similar patterns of localization were observed for C-terminally AcGFP1-tagged $G\alpha_{o1}$ (Figure S1). These localization patterns suggest that the function of the p.Thr191_Phe197del altered protein might be most severely affected.

Structural Impacts of the Mutations on the Gα-Containing Complexes

To evaluate the impact of the *GNAO1* mutations on specific functions at the atomic level, we mapped the substituted positions onto structures of the Gα subunit in complexed states representing the GDP-bound inactive state, the nucleotide-free $G\alpha_s\beta\gamma$ in complex with the receptor, and the GTP-bound active state. In the case of point mutations, we further estimated free-energy changes of the mutations by using FoldX software (version 3.0β5).[19]

The region corresponding to amino acid residues 191–197 of human $G\alpha_{o1}$ is located in β strands and their connecting loop region and is involved in interactions with the G-protein-coupled receptor (GPCR) in the $G\alpha\beta\gamma$-β2AR complex (Figure 4A and Figure S2A). Thus, the deletion would affect secondary structure of the molecule and would not only impair the interaction with GPCR but also severely destabilize the Gα-subunit fold. The substituted residues corresponding to Asp174 and Ile279 of the human $G\alpha_{o1}$ subunit are both buried inside the protein (Figure 4A) and are involved in hydrogen-bonding and hydrophobic interactions, respectively (Figure S2B). Therefore, the p.Asp174Gly and p.Ile279Asn substitutions would destabilize the Gα-subunit fold, as supported by FoldX calculations showing a more than 2 kcal/mol increase in free-energy changes for these substitutions (Figure 4B). It can be speculated that these altered proteins tend to be misfolded or denatured in N2A cells and thus have altered cellular localization (Figure 3).

The substituted residue corresponding to Gly203 of human $G\alpha_{o1}$ is located within the highly conserved switch II region, responsible for activation of downstream effectors upon GTP binding (Figure 4A). Conformations of the switch regions differ depending on the complex state of the G protein. In the $G\alpha\beta\gamma$ heterotrimer and the GDP^+ AlF_4^--bound Gα-effector (PLCβ) complex, the glycine residues are closely surrounded by the switch I region and GTP (Figure 4A and Figure S2C). Thus, the p.Gly203Arg substitution would cause steric hindrance between the arginine side chain and the switch I region and/or GTP, destabilizing the complex, as supported by the FoldX calculations showing a remarkable increase in free-energy change upon the p.Gly203Arg substitution. By contrast, in the $G\alpha\beta\gamma$-receptor (β2AR) complex, no substantial steric hindrance was predicted from the structural modeling and FoldX calculations (Figure 4B and Figure S2C). These findings suggest that the p.Gly203Arg-substituted Gα subunit would impair GTP binding and/or activation of the downstream effectors, although it might still bind to GPCR. This prediction was supported by previous reports, in which GTP binding was weakened in the p.Gly203Thr altered Gα.[17] This also appears to be consistent with the apparently normal cellular localization of the p.Gly203Arg altered protein in N2A cells (Figure 3).

Electrophysiological Evaluation of $G\alpha_{o1}$ Mutants

It has been reported that N-type calcium channels are inhibited, at least in part, via $G\alpha_o$-mediated signaling.[7] Using NG108-15 cells, in which norepinephrine-induced calcium-current inhibition is mediated by $G\alpha_o$ (Figure 5A),[29] we analyzed functional properties of altered $G\alpha_{o1}$. Compared with cells expressing WT $G\alpha_{o1}$ (the

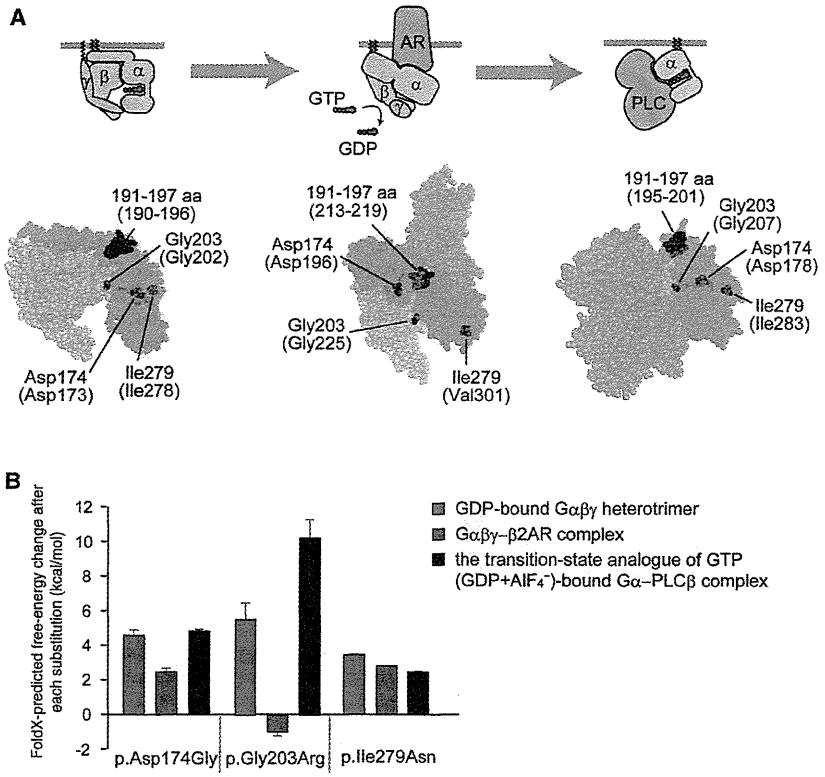

Figure 4. Structural Consideration of the Gα Amino Acid Substitutions in Some Complexed States

(A) Map of the amino acid substitution sites on the crystal structures of Gα-containing complexes: the GDP-bound inactive $G\alpha_i\beta\gamma$ heterotrimer (left), the nucleotide-free $G\alpha_s\beta\gamma$ in complex with an agonist-occupied monomeric β2AR (center), and the $GDP^+AlF_4^-$-bound $G\alpha_q$ in complex with its effector PLCβ (right). Molecular structures are shown as space-filling representations (from PyMOL). Gα, Gβ, and Gγ subunits are colored green, yellow, and pink, respectively, and the switch I and switch II regions in the Gα subunit are in light green. The β2AR (center) and PLCβ (right) molecules are colored brown. The substituted sites are shown in red, and the indicated amino acid numbers correspond to human $G\alpha o_1$ and, in parentheses, rat $G\alpha i_1$ (UniProtKB/Swiss-Prot P10824) (left), bovine Gαs (UniProtKB/Swiss-Prot P04896) (center), and mouse Gαq (UniProtKB/Swiss-Prot P21279) (right). The illustrations above each model show the orientation of each subunit and the bound molecules.

(B) The free-energy change after each of the amino acid substitutions was estimated from calculations using FoldX software. Each error bar represents an average value with a SD.

leftmost column in Figure 5B), NG108-15 cells expressing the p.Thr191_Phe197del substitution revealed a significant increase in calcium-current density before application of norepinephrine ($p < 0.05$ by Dunnett's post hoc test; the second column from the right in Figure 5B), suggesting that localization of the altered $G\alpha_{o1}$ might affect calcium-channel activity. In cells expressing the p.Asp174Gly substitution, a mild increase in the current density was also suggested, although the difference was not significant (the third column from the left in Figure 5B). The other two substitutions had no effects on the current (the second column from the left and the rightmost column in Figure 5B). Treatment with 10 μM norepinephrine reduced the calcium-current density by 19.0% ± 5.0% in cells expressing WT $G\alpha_{o1}$ ($p < 0.01$ by paired t test; left panel in Figure 5A and the leftmost bar in Figure 5C). A similar reduction was observed in cells expressing the p.Ile279Asn alteration (18.5% ± 3.5%, $p < 0.01$ by paired t test; the rightmost bar in Figure 5C). In cells expressing the p.Thr191_Phe197del alteration, by contrast, the reduction was obscured (12.1% ± 5.0%, not significant by paired t test; right panel in Figure 5A and the second bar from the right in Figure 5C). In cells expressing the other two substitutions (p.Gly203Thr and p.Asp174Gly), weaker current inhibition by norepinephrine was suggested (9.9% ± 3.8% and 11.1% ± 3.5%, respectively; both were $p < 0.05$ by paired t test; the second and third bars from the left in Figure 5C), although compared with that in WT-expressing cells, the degrees of inhibition in Gly203Thr- and p.Asp174Gly-expressing cells did not reach statistical significance (not significant by ANOVA). These data suggest that *GNAO1* mutations could hamper $G\alpha_o$-mediated signaling.

Discussion

We successfully identified four de novo heterozygous missense *GNAO1* mutations in four individuals. All four individuals showed severe intellectual disability and motor developmental delay, demonstrating that aberration of $G\alpha_o$ affects intellectual and motor development. In addition, all four individuals showed epileptic encephalopathy, and two of them showed involuntary movements. Because $G\alpha_o$-deficient mice show occasional seizures and generalized tremor,[9,10] it is likely that epilepsy and involuntary movement are two of the characteristic features caused by *GNAO1* mutations. Although $G\alpha_o$-deficient mice also show hyperactivity and hyperalgesia,[10] it is difficult to evaluate whether our individuals had these symptoms because of severe motor and cognitive impairment.

All four of these mutations, and especially two mutations leading to the p.Thr191_Phe197del and p.Gly203Arg substitutions, are predicted to affect $G\alpha_o$ function by structural evaluation. In fact, transient expression in N2A cells showed that localization of the p.Thr191_Phe197del altered protein was dramatically changed to the cytosolic compartment. Interestingly, two alterations (p.Ile279Asn

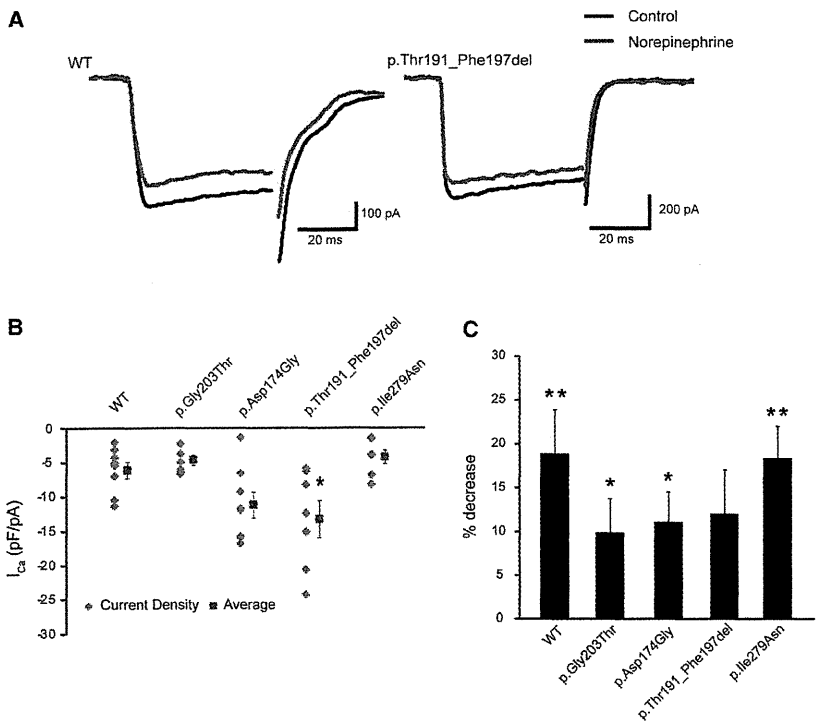

Figure 5. Evaluation of $G\alpha_o$-Mediated Signaling in NG108-15 Cell Calcium-Current Generation

(A) Representative traces of voltage-gated calcium currents generated in NG108-15 cells expressing WT (left) or p.Thr191_Phe197del altered (right) $G\alpha_{o1}$. Black and red traces represent the currents before and 3 min after application of 10 μM norepinephrine, respectively.

(B) Current densities of the calcium currents before norepinephrine treatment in cells expressing WT or altered $G\alpha_{o1}$. Scatter plots represent the densities in individual cells. Red squares and bars represent the means and SEMs, respectively, of the densities in individual cell groups (WT, n = 8; p.Gly203Thr, n = 7; p.Asp174Gly, n = 8; p.Thr191_Phe197del, n = 7; p.Ile279Asn, n = 7). Compared with that in cells expressing WT $G\alpha_{o1}$, the current density in cells expressing p.Thr191_Phe197del increased significantly (*$p < 0.05$ by Dunnett's post hoc test). The densities in the cells expressing other altered proteins did not vary significantly.

(C) Comparison of norepinephrine-induced inhibition of calcium currents in cells expressing altered $G\alpha_{o1}$. Each error bar represents the mean and SEM of the percent decrease in current density induced by application of 10 μM norepinephrine. Paired t tests indicated that the inhibition induced by norepinephrine was significant in cells expressing WT (n = 8) and p.Gly203Thr (n = 7), p.Asp174Gly (n = 8), and p.Ile279Asn (n = 7) altered proteins (**$p < 0.01$ and *$p < 0.05$), but not in cells expressing p.Thr191_Phe197del (n = 7). Although there was some tendency for decreased inhibition in cells expressing altered proteins, the tendency did not reach statistical significance compared with that in WT-expressing cells ($p = 0.41$ by ANOVA).

and p.Asp174Gly) also showed weak signal in the cytosol, suggesting that localization to the plasma membrane was variably impaired in three altered proteins. Measurement of voltage-dependent calcium currents in NG108-15 cells also suggested impaired functions of altered $G\alpha_{o1}$. The p.Thr191_Phe197del alteration significantly increased the basal calcium-current density, and compared with WT-expressing cells, cells expressing one of the three substitutions (p.Thr191_Phe197del, p.Asp174Gly, or p.Gly203Thr) showed a tendency towards weaker inhibition of calcium currents by norepinephrine. All these data suggest that the four *GNAO1* mutations might cause loss of $G\alpha_{o1}$ function.

Our experimental data suggest that $G\alpha_o$ function might be most severely affected in the p.Thr191_Phe197del altered protein. This appears to be correlated with the severity of clinical features because individual 3 showed both OS and involuntary movements and indeed died during the infantile period. Therefore, she might have had the most severe phenotype caused by a *GNAO1* mutation. Another interesting finding is somatic mosaicism of the c.521A>G (p.Asp174Gly) mutation in individual 2, in whom approximately 35%–50% of cells harbored the mutation. Somatic mosaicism of responsive genes in infantile epilepsy, such as *SCN1A* (MIM 182389) and *STXBP1*, have been reported, explaining the presence of unaffected or mildly affected transmitting parents.[30,31] However, individual 2 showed OS, delayed myelination, and thin corpus callosum. Although we did not determine the mosaic rate in brain tissues, the presence of 35%–50% of cells harboring the *GNAO1* mutation in the brain might be sufficient to cause abnormal brain development.

It has been reported that activation of G-protein-coupled α_2 adrenergic receptors by norepinephrine attenuates epileptiform activity in the hippocampal CA3 region.[32] $G\alpha_o$ is known to be involved in this response,[33] suggesting that alteration of pathways mediated by α_2 adrenergic receptor and $G\alpha_o$ might contribute to the pathogenesis of epilepsy. Because calcium-current inhibition is a well-known consequence of $G\alpha_o$-mediated signaling induced by norepinephrine, it is possible that epileptic seizures associated with *GNAO1* mutations might be improved by calcium-channel modulators. For example, pregabalin and gabapentin act as selective calcium-channel blockers,[34,35] and topiramate modulates high-voltage-activated calcium channels in dentate granule cells.[36] Because our four individuals were not treated with these drugs, it is worth administrating these three drugs for examining putative protective effects.

In conclusion, de novo heterozygous *GNAO1* mutations were identified in four individuals with epileptic encephalopathy. Furthering our understanding of abnormal

$G\alpha_o$-mediated heterotrimeric G protein signaling might provide new insights into the pathogenesis and treatment of epileptic encephalopathy.

Supplemental Data

Supplemental Data include two figures, three tables, and one movie and can be found with this article online at http://www.cell.com/AJHG.

Acknowledgments

We would like to thank the individuals and their families for their participation in this study. We also thank Aya Narita and Nobuko Watanabe for their technical assistance and Tohru Kozasa and Nobuchika Suzuki for their valuable comments. This work was supported by the Ministry of Health, Labour, and Welfare of Japan, the Japan Society for the Promotion of Science (Grants-in-Aid for Scientific Research (B) [25293085 and 25293235] and a Grant-in-Aid for Scientific Research (A) [13313587]), the Takeda Science Foundation, the Japan Science and Technology Agency, the Strategic Research Program for Brain Sciences (11105137), and a Grant-in-Aid for Scientific Research on Innovative Areas (Transcription Cycle) from the Ministry of Education, Culture, Sports, Science, and Technology of Japan (12024421).

Received: May 17, 2013
Revised: July 9, 2013
Accepted: July 17, 2013
Published: August 29, 2013

Web Resources

The URLs for data presented herein are as follows:

CLUSTALW, http://www.genome.jp/tools/clustalw/
GenBank, http://www.ncbi.nlm.nih.gov/Genbank/
NHLBI Exome Sequencing Project (ESP) Exome Variant Server, http://evs.gs.washington.edu/EVS/
Online Mendelian Inheritance in Man (OMIM), http://www.omim.org/
Picard, http://picard.sourceforge.net/
Protein Data Bank, http://www.rcsb.org/pdb/home/home.do
PyMOL, www.pymol.org
RefSeq, http://www.ncbi.nlm.nih.gov/RefSeq
UniProtKB/Swiss-Prot, http://www.uniprot.org/

References

1. Dulac, O. (2001). Epileptic encephalopathy. Epilepsia *42* (*Suppl 3*), 23–26.
2. Ohtahara, S., and Yamatogi, Y. (2006). Ohtahara syndrome: with special reference to its developmental aspects for differentiating from early myoclonic encephalopathy. Epilepsy Res. *70* (*Suppl 1*), S58–S67.
3. Saitsu, H., Kato, M., Koide, A., Goto, T., Fujita, T., Nishiyama, K., Tsurusaki, Y., Doi, H., Miyake, N., Hayasaka, K., and Matsumoto, N. (2012). Whole exome sequencing identifies *KCNQ2* mutations in Ohtahara syndrome. Ann. Neurol. *72*, 298–300.
4. Saitsu, H., Kato, M., Mizuguchi, T., Hamada, K., Osaka, H., Tohyama, J., Uruno, K., Kumada, S., Nishiyama, K., Nishimura, A., et al. (2008). *De novo* mutations in the gene encoding STXBP1 (MUNC18-1) cause early infantile epileptic encephalopathy. Nat. Genet. *40*, 782–788.
5. Weckhuysen, S., Mandelstam, S., Suls, A., Audenaert, D., Deconinck, T., Claes, L.R., Deprez, L., Smets, K., Hristova, D., Yordanova, I., et al. (2012). *KCNQ2* encephalopathy: emerging phenotype of a neonatal epileptic encephalopathy. Ann. Neurol. *71*, 15–25.
6. Kato, M., Saitoh, S., Kamei, A., Shiraishi, H., Ueda, Y., Akasaka, M., Tohyama, J., Akasaka, N., and Hayasaka, K. (2007). A longer polyalanine expansion mutation in the *ARX* gene causes early infantile epileptic encephalopathy with suppression-burst pattern (Ohtahara syndrome). Am. J. Hum. Genet. *81*, 361–366.
7. Wettschureck, N., and Offermanns, S. (2005). Mammalian G proteins and their cell type specific functions. Physiol. Rev. *85*, 1159–1204.
8. Huff, R.M., Axton, J.M., and Neer, E.J. (1985). Physical and immunological characterization of a guanine nucleotide-binding protein purified from bovine cerebral cortex. J. Biol. Chem. *260*, 10864–10871.
9. Valenzuela, D., Han, X., Mende, U., Fankhauser, C., Mashimo, H., Huang, P., Pfeffer, J., Neer, E.J., and Fishman, M.C. (1997). G alpha(o) is necessary for muscarinic regulation of Ca2+ channels in mouse heart. Proc. Natl. Acad. Sci. USA *94*, 1727–1732.
10. Jiang, M., Gold, M.S., Boulay, G., Spicher, K., Peyton, M., Brabet, P., Srinivasan, Y., Rudolph, U., Ellison, G., and Birnbaumer, L. (1998). Multiple neurological abnormalities in mice deficient in the G protein Go. Proc. Natl. Acad. Sci. USA *95*, 3269–3274.
11. Saitsu, H., Kato, M., Osaka, H., Moriyama, N., Horita, H., Nishiyama, K., Yoneda, Y., Kondo, Y., Tsurusaki, Y., Doi, H., et al. (2012). *CASK* aberrations in male patients with Ohtahara syndrome and cerebellar hypoplasia. Epilepsia *53*, 1441–1449.
12. Saitsu, H., Nishimura, T., Muramatsu, K., Kodera, H., Kumada, S., Sugai, K., Kasai-Yoshida, E., Sawaura, N., Nishida, H., Hoshino, A., et al. (2013). *De novo* mutations in the autophagy gene *WDR45* cause static encephalopathy of childhood with neurodegeneration in adulthood. Nat. Genet. *45*, 445–449, e1.
13. DePristo, M.A., Banks, E., Poplin, R., Garimella, K.V., Maguire, J.R., Hartl, C., Philippakis, A.A., del Angel, G., Rivas, M.A., Hanna, M., et al. (2011). A framework for variation discovery and genotyping using next-generation DNA sequencing data. Nat. Genet. *43*, 491–498.
14. Wang, K., Li, M., and Hakonarson, H. (2010). ANNOVAR: functional annotation of genetic variants from high-throughput sequencing data. Nucleic Acids Res. *38*, e164.
15. Robinson, J.T., Thorvaldsdóttir, H., Winckler, W., Guttman, M., Lander, E.S., Getz, G., and Mesirov, J.P. (2011). Integrative genomics viewer. Nat. Biotechnol. *29*, 24–26.
16. Thorvaldsdóttir, H., Robinson, J.T., and Mesirov, J.P. (2013). Integrative Genomics Viewer (IGV): high-performance genomics data visualization and exploration. Brief. Bioinform. *14*, 178–192.
17. Slepak, V.Z., Wilkie, T.M., and Simon, M.I. (1993). Mutational analysis of G protein alpha subunit G(o) alpha expressed in Escherichia coli. J. Biol. Chem. *268*, 1414–1423.
18. Williams, D.J., Puhl, H.L., and Ikeda, S.R. (2010). A Simple, Highly Efficient Method for Heterologous Expression in Mammalian Primary Neurons Using Cationic Lipid-mediated mRNA Transfection. Front Neurosci. *4*, 181.

19. Guerois, R., Nielsen, J.E., and Serrano, L. (2002). Predicting changes in the stability of proteins and protein complexes: a study of more than 1000 mutations. J. Mol. Biol. *320*, 369–387.
20. Wall, M.A., Coleman, D.E., Lee, E., Iñiguez-Lluhi, J.A., Posner, B.A., Gilman, A.G., and Sprang, S.R. (1995). The structure of the G protein heterotrimer Gi alpha 1 beta 1 gamma 2. Cell *83*, 1047–1058.
21. Rasmussen, S.G., DeVree, B.T., Zou, Y., Kruse, A.C., Chung, K.Y., Kobilka, T.S., Thian, F.S., Chae, P.S., Pardon, E., Calinski, D., et al. (2011). Crystal structure of the β2 adrenergic receptor-Gs protein complex. Nature *477*, 549–555.
22. Waldo, G.L., Ricks, T.K., Hicks, S.N., Cheever, M.L., Kawano, T., Tsuboi, K., Wang, X., Montell, C., Kozasa, T., Sondek, J., and Harden, T.K. (2010). Kinetic scaffolding mediated by a phospholipase C-beta and Gq signaling complex. Science *330*, 974–980.
23. Edvardson, S., Baumann, A.M., Mühlenhoff, M., Stephan, O., Kuss, A.W., Shaag, A., He, L., Zenvirt, S., Tanzi, R., Gerardy-Schahn, R., and Elpeleg, O. (2013). West syndrome caused by ST3Gal-III deficiency. Epilepsia *54*, e24–e27.
24. Molinari, F., Raas-Rothschild, A., Rio, M., Fiermonte, G., Encha-Razavi, F., Palmieri, L., Palmieri, F., Ben-Neriah, Z., Kadhom, N., Vekemans, M., et al. (2005). Impaired mitochondrial glutamate transport in autosomal recessive neonatal myoclonic epilepsy. Am. J. Hum. Genet. *76*, 334–339.
25. Mills, P.B., Surtees, R.A., Champion, M.P., Beesley, C.E., Dalton, N., Scambler, P.J., Heales, S.J., Briddon, A., Scheimberg, I., Hoffmann, G.F., et al. (2005). Neonatal epileptic encephalopathy caused by mutations in the PNPO gene encoding pyridox(am)ine 5′-phosphate oxidase. Hum. Mol. Genet. *14*, 1077–1086.
26. Shen, J., Gilmore, E.C., Marshall, C.A., Haddadin, M., Reynolds, J.J., Eyaid, W., Bodell, A., Barry, B., Gleason, D., Allen, K., et al. (2010). Mutations in PNKP cause microcephaly, seizures and defects in DNA repair. Nat. Genet. *42*, 245–249.
27. Kurian, M.A., Meyer, E., Vassallo, G., Morgan, N.V., Prakash, N., Pasha, S., Hai, N.A., Shuib, S., Rahman, F., Wassmer, E., et al. (2010). Phospholipase C beta 1 deficiency is associated with early-onset epileptic encephalopathy. Brain *133*, 2964–2970.
28. Nakata, H., and Kozasa, T. (2005). Functional characterization of Galphao signaling through G protein-regulated inducer of neurite outgrowth 1. Mol. Pharmacol. *67*, 695–702.
29. McFadzean, I., Mullaney, I., Brown, D.A., and Milligan, G. (1989). Antibodies to the GTP binding protein, Go, antagonize noradrenaline-induced calcium current inhibition in NG108-15 hybrid cells. Neuron *3*, 177–182.
30. Saitsu, H., Hoshino, H., Kato, M., Nishiyama, K., Okada, I., Yoneda, Y., Tsurusaki, Y., Doi, H., Miyake, N., Kubota, M., et al. (2011). Paternal mosaicism of an *STXBP1* mutation in OS. Clin. Genet. *80*, 484–488.
31. Marini, C., Scheffer, I.E., Nabbout, R., Suls, A., De Jonghe, P., Zara, F., and Guerrini, R. (2011). The genetics of Dravet syndrome. Epilepsia *52* (*Suppl 2*), 24–29.
32. Jurgens, C.W., Hammad, H.M., Lichter, J.A., Boese, S.J., Nelson, B.W., Goldenstein, B.L., Davis, K.L., Xu, K., Hillman, K.L., Porter, J.E., and Doze, V.A. (2007). Alpha2A adrenergic receptor activation inhibits epileptiform activity in the rat hippocampal CA3 region. Mol. Pharmacol. *71*, 1572–1581.
33. Goldenstein, B.L., Nelson, B.W., Xu, K., Luger, E.J., Pribula, J.A., Wald, J.M., O'Shea, L.A., Weinshenker, D., Charbeneau, R.A., Huang, X., et al. (2009). Regulator of G protein signaling protein suppression of Galphao protein-mediated alpha2A adrenergic receptor inhibition of mouse hippocampal CA3 epileptiform activity. Mol. Pharmacol. *75*, 1222–1230.
34. Sills, G.J. (2006). The mechanisms of action of gabapentin and pregabalin. Curr. Opin. Pharmacol. *6*, 108–113.
35. Stefani, A., Spadoni, F., Giacomini, P., Lavaroni, F., and Bernardi, G. (2001). The effects of gabapentin on different ligand- and voltage-gated currents in isolated cortical neurons. Epilepsy Res. *43*, 239–248.
36. Zhang, X., Velumian, A.A., Jones, O.T., and Carlen, P.L. (2000). Modulation of high-voltage-activated calcium channels in dentate granule cells by topiramate. Epilepsia *41* (*Suppl 1*), S52–S60.

RESEARCH ARTICLE

Human Mutation

OFFICIAL JOURNAL
HGVS
HUMAN GENOME VARIATION SOCIETY
www.hgvs.org

De Novo Mutations in *SLC35A2* Encoding a UDP-Galactose Transporter Cause Early-Onset Epileptic Encephalopathy

Hirofumi Kodera,[1†] Kazuyuki Nakamura,[1,2†] Hitoshi Osaka,[3] Yoshihiro Maegaki,[4] Kazuhiro Haginoya,[5,6] Shuji Mizumoto,[7] Mitsuhiro Kato,[2] Nobuhiko Okamoto,[8] Mizue Iai,[3] Yukiko Kondo,[1] Kiyomi Nishiyama,[1] Yoshinori Tsurusaki,[1] Mitsuko Nakashima,[1] Noriko Miyake,[1] Kiyoshi Hayasaka,[2] Kazuyuki Sugahara,[7] Isao Yuasa,[9] Yoshinao Wada,[10] Naomichi Matsumoto,[1]* and Hirotomo Saitsu[1]**

[1]Department of Human Genetics, Yokohama City University Graduate School of Medicine, Kanazawa-ku, Yokohama 236-0004, Japan; [2]Department of Pediatrics, Yamagata University School of Medicine, Yamagata 990-9585, Japan; [3]Division of Neurology, Clinical Research Institute, Kanagawa Children's Medical Center, Minami-ku, Yokohama 232-8555, Japan; [4]Division of Child Neurology, Faculty of Medicine, Tottori University, Yonago 683-8504, Japan; [5]Department of Pediatrics, Tohoku University School of Medicine, Aoba-ku, Sendai 980-8574, Japan; [6]Department of Pediatric Neurology, Takuto Rehabilitation Center for Children, Taihaku-ku, Sendai 982-0241, Japan; [7]Laboratory of Proteoglycan Signaling and Therapeutics, Frontier Research Center for Post-Genomic Science and Technology, Graduate School of Life Science, Hokkaido University, Sapporo 001-0021, Japan; [8]Department of Medical Genetics, Osaka Medical Center and Research Institute for Maternal and Child Health, Izumi, Osaka 594-1101, Japan; [9]Division of Legal Medicine, Faculty of Medicine, Tottori University, Yonago 683-8503, Japan; [10]Department of Molecular Medicine, Osaka Medical Center and Research Institute for Maternal and Child Health, Izumi, Osaka 594-1101, Japan

Communicated by María-Jesús Sobrido

Received 16 May 2013; accepted revised manuscript 15 September 2013.
Published online 30 September 2013 in Wiley Online Library (www.wiley.com/humanmutation). DOI: 10.1002/humu.22446

ABSTRACT: Early-onset epileptic encephalopathies (EOEE) are severe neurological disorders characterized by frequent seizures accompanied by developmental regression or retardation. Whole-exome sequencing of 12 patients together with five pairs of parents and subsequent Sanger sequencing in additional 328 EOEE patients identified two de novo frameshift and one missense mutations in *SLC35A2* at Xp11.23, respectively. The three patients are all females. X-inactivation analysis of blood leukocyte DNA and mRNA analysis using lymphoblastoid cells derived from two patients with a frameshift mutation indicated that only the wild-type *SLC35A2* allele was expressed in these cell types, at least in part likely as a consequence of skewed X-inactivation. *SLC35A2* encodes a UDP-galactose transporter (UGT), which selectively supplies UDP-galactose from the cytosol to the Golgi lumen. Transient expression experiments revealed that the missense mutant protein was correctly localized in the Golgi apparatus. In contrast, the two frameshift mutant proteins were not properly expressed, suggesting that their function is severely impaired. Defects in the UGT can cause congenital disorders of glycosylation. Of note, no abnormalities of glycosylation were observed in three serum glycoproteins, which is consistent with favorably skewed X-inactivation. We hypothesize that a substantial number of neurons might express the mutant *SLC35A2* allele and suffer from defective galactosylation, resulting in EOEE.
Hum Mutat 34:1708–1714, 2013. © 2013 Wiley Periodicals, Inc.

KEY WORDS: early-onset epileptic encephalopathy; *SLC35A2*; congenital disorders of glycosylation

Introduction

Glycosylation is the process of adding complex sugar chains (glycans) to proteins and lipids. Protein glycosylation includes *N*-linked and *O*-linked glycosylation pathways in the endoplasmic reticulum (ER)–Golgi network [Freeze, 2013]. To enable glycan biosynthesis, monosaccharides in the form of nucleotide sugars, such as GDP-fucose, CMP-sialic acid, and UDP-galactose, must be delivered into the lumen of the ER and Golgi apparatus by their respective nucleotide-sugar transporters [Liu et al., 2010]. Defects of the glycosylation process cause congenital disorders of glycosylation (CDG). To date, nearly 70 CDG have been identified, most caused by either the *N*-linked or *O*-linked glycosylation pathway, or both [Freeze, 2013; Jaeken and Matthijs, 2007]. Because glycosylation is a ubiquitous cellular process, its defects affect multiple organ systems with various features, accompanied by facial dysmorphism. The central nervous system is one of the most often affected organs, frequently resulting in structural abnormalities, developmental delay, and epileptic seizures [Freeze et al., 2012].

Additional Supporting Information may be found in the online version of this article.

†These authors contributed equally to this work.

*Correspondence to: Naomichi Matsumoto. Department of Human Genetics, Yokohama City University Graduate School of Medicine, 3-9 Fukuura, Kanazawa-ku, Yokohama 236-0004, Japan. E-mail: naomat@yokohama-cu.ac.jp

**Correspondence to: Hirotomo Saitsu. Department of Human Genetics, Yokohama City University Graduate School of Medicine, 3-9 Fukuura, Kanazawa-ku, Yokohama 236-0004, Japan. E-mail: hsaitsu@yokohama-cu.ac.jp

Contract grant sponsors: Ministry of Health, Labour, and Welfare of Japan; the Japan Society for the Promotion of Science (Grant-in-Aid for Scientific Research B [25293085], [25293235], Grant-in-Aid for Scientific Research A [13313587]); Takeda Science Foundation; Japan Science and Technology Agency; Strategic Research Program for Brain Sciences (11105137); Grants-in-Aid for Scientific Research on Innovative Areas (Transcription Cycle, Neuroglycobiology) from the Ministry of Education, Culture, Sports, Science, and Technology of Japan (12024421, 24110501).

Early-onset epileptic encephalopathies (EOEE), with onset before 1 year of age, are characterized by severe seizures (often). infantile spasms), frequent interictal epileptiform activity on a disorganized electroencephalogram (EEG) background, and developmental regression or retardation [Holland and Hallinan, 2010]. Ohtahara syndrome (MIMs # 308350, 612164), West syndrome (WS; MIMs # 308350, 300672, 612164), early myoclonic epileptic encephalopathy (MIM #609304), malignant migrating partial seizures of infancy (MIM #614959), and Dravet syndrome (MIM #607208) are the best known epileptic encephalopathies recognized by the International League Against Epilepsy. However, many infants with these syndromes do not strictly fit within the electroclinical parameters of these syndromes. Recently, several causative genes have been reported in patients both with well-recognized and unclassified EOEE syndromes: *ARX* (MIM #300382), *CDKL5* (MIM #300203), *STXBP1* (MIM #602926), *SLC25A22* (MIM #609302), *SCN1A* (MIM #182389), *KCNQ2* (MIM #602235), and *KCNT1* (MIM #608167) [Barcia et al., 2012; Claes et al., 2001; Kalscheuer et al., 2003; Kato et al., 2007; Molinari et al., 2005; Saitsu et al., 2008, 2012a; Stromme et al., 2002; Weckhuysen et al., 2012]. These genes encode sodium or potassium channels, transcription factors, a mitochondrial glutamate transporter, and a regulator of neurotransmitter release, and are able to explain part of the genetic cause of EOEE. Because epileptic seizures are one of the main symptoms with CDG, abnormal glycosylation may be found in EOEE. In fact, de novo mutations in *SLC35A2* (MIM #314375), encoding a UDP-galactose transporter (UGT), have recently been reported in three patients with CDG (one female with a heterozygous mutation and two males with a mosaic mutation), and two of them showed seizures and hypsarrhythmia on EEG, suggesting WS [Ng et al., 2013]. It would be worth checking *SLC35A2* mutations in a large cohort of patients with EOEE.

In this study, whole-exome sequencing (WES) of 12 patients together with five pairs of parents (five trios) and subsequent Sanger sequencing in additional 328 patients with EOEE identified two de novo frameshift and one de novo missense mutations in *SLC35A2*, respectively, confirming that de novo *SLC35A2* mutations are one of the genetic causes for EOEE.

Materials and Methods

Methods for RNA analysis, X-inactivation analysis, and mass spectrometry are described in the Supp. Methods.

Patients

A total of 328 patients with EOEE (67 patients with Ohtahara syndrome, 150 with WS, and 111 with unclassified EOEE) were analyzed for *SLC35A2* mutations. The diagnosis was made based on clinical features and characteristic patterns on EEG. In 257 patients, mutations in *STXBP1* and *KCNQ2* had been excluded by high-resolution melting analysis in advance. Experimental protocols were approved by the Institutional Review Board of Yokohama City University School of Medicine. Clinical information and peripheral blood samples were obtained from the family members after obtaining written informed consent.

Exome Sequencing

WES for 12 patients with EOEE, in whom initial diagnosis was Ohtahara syndrome, had been previously performed [Saitsu et al., 2012a, 2012b]. In this study, we additionally analyzed parental samples from five patients by WES. Genomic DNA was captured using the SureSelectXT Human All Exon v4 Kit (Agilent Technologies, Santa Clara, CA) and sequenced with four samples per lane on an Illumina HiSeq 2000 (Illumina, San Diego, CA) with 101-bp paired-end reads. Image analysis and base calling were performed by sequence control software with real-time analysis and CASAVA software v1.8 (Illumina). Exome data processing, variant calling, and variant annotation were performed as previously described [DePristo et al., 2011; Saitsu et al., 2013; Wang et al., 2010]. All de novo candidate mutations detected by WES were confirmed by Sanger sequencing.

Mutation Screening

Genomic DNA was amplified using an illustra GenomiPhi V2 DNA Amplification Kit (GE Healthcare, Buckinghamshire, UK). Exons 1–5 covering the *SLC35A2* coding region of two transcript variants (transcript variant 1, GenBank accession number NM_005660.1, encoding UGT2; transcript variant 3, GenBank accession number NM_001042498.2, encoding UGT1) were screened by Sanger sequencing. PCR primers and conditions are available on request. All novel mutations were verified using original genomic DNA, and searched for in the variant database of our 408 in-house control exomes.

Expression Vectors

Total RNA from lymphoblastoid cells was reverse transcribed using the PrimeScript 1st strand synthesis kit with random hexamers (Takara, Ohtsu, Japan) as previously reported [Saitsu et al., 2010]. The following primers were used to isolate full-length human *SLC35A2* cDNA (amino acids 1–393, GenBank accession number NM_001042498.2): forward 5′-GGAATTCAGATGCCAACATGGCAGCGGTTGG–3′ and reverse 5′-GGCTCGAGATTGCTGCCAGCCCTCACTTCAC–3′. *SLC35A2* cDNA was inserted into pBlueScript SK(-) vector (Agilent Technologies), and site-directed mutagenesis was performed using a KOD-Plus-Mutagenesis kit (Toyobo, Osaka, Japan) according to the manufacturer's protocol to generate *SLC35A2* mutants including c.433_434del (p.Tyr145Profs*76), c.972del (p.Phe324Leufs*25), and c.638C>T (p.Ser213Phe). Subsequently, mutant *SLC35A2* cDNAs that excluded termination codons were amplified by PCR, inserted into pEF6/V5-His C vector (Life Technologies Co., Carlsbad, CA) to generate C terminal V5-epitope tag. All variant cDNAs were confirmed by Sanger sequencing.

Cell Culture

Mouse neuroblastoma 2A (N2A) cells were cultured at 37°C under 5% CO_2 in DMEM, high glucose, GlutaMAX(™) supplemented with 10% fetal bovine serum and Penicillin–Streptomycin (Life Technologies Co.).

Immunofluorescence Microscopy

N2A cells on glass cover slips were transfected with 200 ng of plasmid DNA using X-tremeGENE 9 DNA Transfection Reagent (Roche Diagnostics, Mannheim, Germany). After 24 hr, cells were fixed in 4% paraformaldehyde/PBS for 15 min and permeabilized in 0.1% Triton X-100/PBS for 5 min. Cells were then blocked with 10% normal goat serum for 30 min. V5-tagged UGT1 were detected by mouse anti-V5 antibody (1:200 dilution; Life Technologies) and Alexa-488-conjugated goat anti-mouse immunoglobulin G (1:1000 dilution; Life Technologies). Cover slips were mounted using

Vectashield (Vector Laboratories, Youngstown, OH) that contained 4′,6-diamidino-2-phenylindole (DAPI) and visualized with an inverted FV1000-D confocal microscope (Olympus, Tokyo, Japan).

Results

To systemically screen de novo or recessive mutations, we conducted trio-based WES in five patients with EOEE. None of the recessive mutations in known EOEE genes were found in WES data (*SLC25A22*, *PNPO*; MIM #610090, *PNKP*; MIM #613402, *PLCB1*; MIM #613722, and *ST3GAL3*; MIM #615006) [Hu et al., 2011; Kurian et al., 2010; Mills et al., 2005; Molinari et al., 2005; Shen et al., 2010]. Instead, we found one or two de novo nonsynonymous mutations in each of the five trios (Supp. Table S1). Among them, a sole de novo frameshift mutation in *SLC35A2* at Xp11.23 was found in two patients: c.433_434del (p.Tyr145Profs*76) in patient 1 and c.972del (p.Phe324Leufs*25) in patient 2, which were confirmed by Sanger sequencing. No *SLC35A2* mutation was found in the other seven patients analyzed by WES. However, subsequent *SLC35A2* mutation analysis by Sanger sequencing in a cohort of 328 patients with EOEE revealed another de novo missense mutation (c.638C>T [p.Ser213Phe]) in patient 3 (Fig. 1A). None of the three mutations was found in the 6,500 National Heart, Lung, and Blood Institute exomes (http://evs.gs.washington.edu/EVS/) or our 408 in-house control exomes. All patients with a *SLC35A2* mutation are female.

As human female cells are subject to X-chromosome inactivation, we examined the X-inactivation pattern using a fragile X mental retardation locus methylation assay and human androgen receptor assay on genomic DNA from peripheral leukocytes [Kondo et al., 2012]. A markedly skewed pattern was observed in patients 1 and 2 (noninformative in patient 3) (Supp. Table S2). Reverse-transcription PCR and sequencing of total RNA extracted from lymphoblastoid cell lines derived from patients 1 and 2 revealed that only the wild-type (WT) *SLC35A2* allele was expressed, suggesting that the mutant alleles underwent X-inactivation, though degradation of mutant transcripts by nonsense-mediated mRNA decay may be involved (Supp. Fig. S1). Cells from patient 3 were unavailable. It is unknown whether the mutant allele undergoes similar X-inactivation in brain tissues.

SLC35A2 encodes a UGT, which selectively supplies UDP-galactose from the cytosol to the Golgi lumen [Ishida et al., 1996; Miura et al., 1996]. Two human UGT splice variants have been studied: UGT1 encoded by transcript variant 3 (NM_001042498.2) and UGT2 by transcript variant 1 (NM_005660.1) [Ishida et al., 1996; Kabuss et al., 2005; Miura et al., 1996], both of which are predicted to have a 10-transmembrane domain and differ only at the carboxyl-terminal five or eight amino acid residues (Fig. 1B) [Kabuss et al., 2005; Miura et al., 1996]. The three mutations would affect both UGT1 and UGT2. Two mutations (p.Tyr145Profs*76 and p.Phe324Leufs*25) would cause truncation of UGT within the transmembrane domain, and the missense mutation (p.Ser213Phe) occurs at an evolutionarily conserved amino acid (Fig. 1B and Supp. Fig. S2). To examine the effect of the three *SLC35A2* mutations, we performed transient expression experiments in N2A cells. C-terminally V5 epitope-tagged WT UGT1 was localized to the Golgi apparatus, similar to endogenous UGT1 [Yoshioka et al., 1997]. The p.Ser213Phe mutant showed a similar expression pattern to

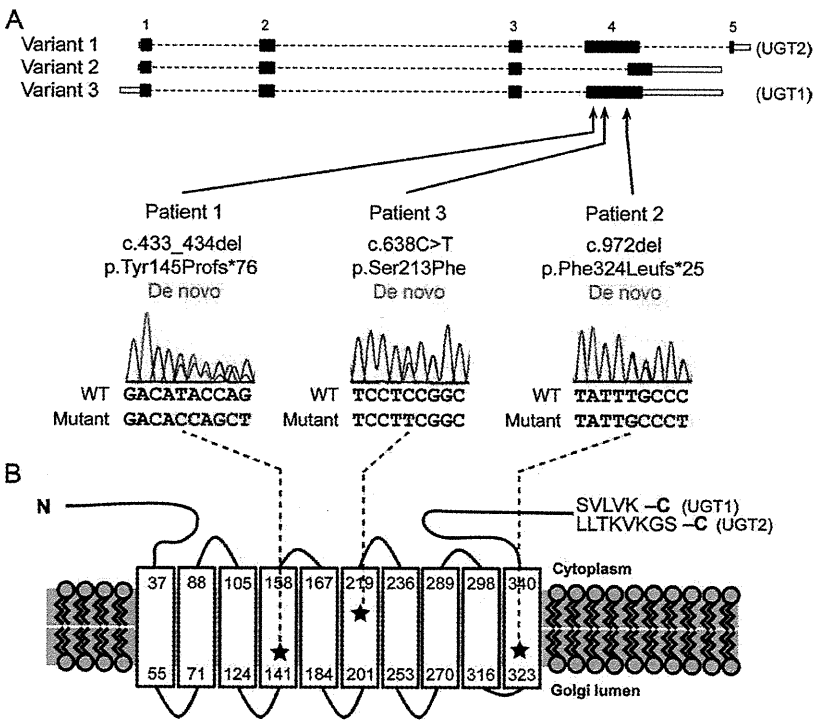

Figure 1. De novo *SLC35A2* mutations in EOEE patients. **A:** Schematic representation of *SLC35A2* (open and filled rectangles represent untranslated regions and coding regions, respectively). There are three transcript variants: variant 1 (GenBank accession number, NM_005660.1) encoding UGT2, variant 2 (NM_005660.1), and variant 3 (NM_001042498.2) encoding UGT1. The three de novo mutations occurred in both variants 1 and 3, but not in variant 2. **B:** Topological prediction of UGT1 and UGT2 proteins [Kabuss et al., 2005]. The three mutations (stars) are predicted to be localized in the transmembrane domains. The C-terminal five amino acids (SVLVK) in UGT1 are replaced by eight amino acids (LLTKVKGS) in UGT2. *SLC35A2* variants were deposited in a gene-specific database (http://databases.lovd.nl/shared/genes/SLC35A2).

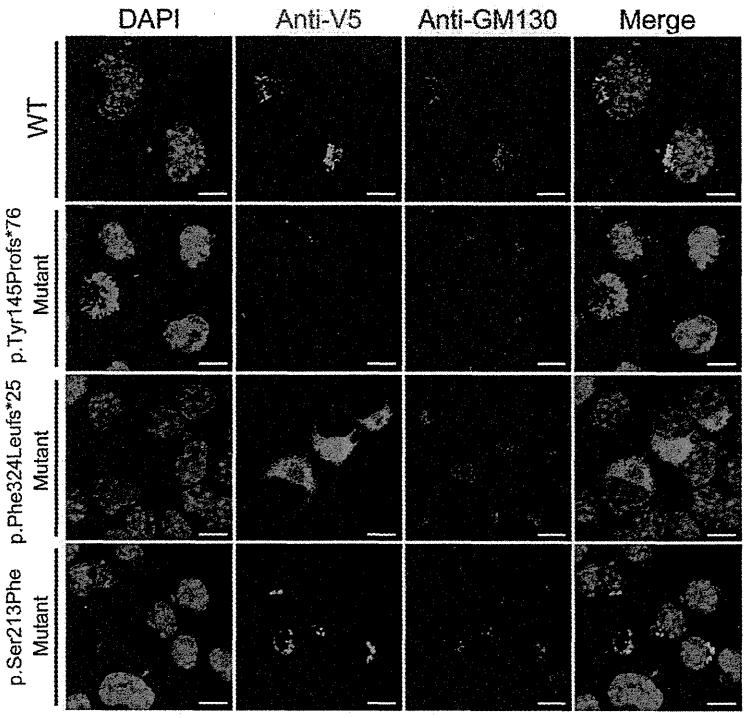

Figure 2. Expression of V5-tagged UGT1 proteins in N2A cells. Expression of WT and the three mutant UGT1 proteins in N2A cells. V5-tagged WT UGT1 (top, green) and the p.Ser213Phe mutant (bottom, green) colocalized with the Golgi marker GM130 (red), suggesting localization to the Golgi apparatus similar to endogenous UGT1. In contrast, the p.Phe324Leufs*25 mutant (lower middle, green) was expressed in the cytosolic compartment, and expression of the p.Tyr145Profs*76 mutant (upper middle, green) was severely diminished. The nucleus was stained with DAPI (blue). The scale bars represent 10 μm.

the WT. In contrast, the p.Phe324Leufs*25 mutant was expressed in the cytosolic compartment and expression of the p.Tyr145Profs*76 mutant was severely diminished, suggesting that the function of the two truncated UGT1 proteins would be severely impaired (Fig. 2).

Because nucleotide-sugar transporters including UGT are critical components of glycosylation pathways such as *N*-glycosylation and *O*-glycosylation in eukaryotes, functional aberration of UGT is likely to affect protein glycosylation [Jaeken, 2003; Liu et al., 2010; Muntoni, 2004; Wopereis et al., 2006]. Therefore, we investigated glycosylation of serum glycoproteins isolated from the patients with a *SLC35A2* mutation, by isoelectric focusing, electrospray ionization, and matrix-assisted laser desorption/ionization mass spectrometry (MALDI-MS) of transferrin and apolipoprotein CIII, and by MALDI-MS of immunoglobulin G (Supp. Figs. S3–S5 and Supp. Table S3). However, we could not detect any abnormalities of *N*-glycosylation or *O*-glycosylation in these serum glycoproteins. Considering that only WT *SLC35A2* is expressed in lymphoblastoid cells from the two patients, these normal glycosylation profiles of serum glycoproteins may be reasonable.

The clinical features of patients with a *SLC35A2* mutation are presented in Table 1. Dysmorphological findings such as thick eyebrows, a broad nasal bridge, thick lips, and maxillary prognathism were found (Fig. 3A–C). Brain magnetic resonance imaging (MRI) showed cerebral and cerebellar atrophy and thinning of the corpus callosum in two patients, 1 and 3, an arachnoid pouch in patient 1, and an enlarged left lateral ventricle in patient 2 (Fig. 3D–H). All patients were diagnosed as WS in their clinical course, and showed no abnormalities in the skin, coagulation, or hepatic enzymes, which are often observed in patients with CDG [Freeze, 2006; Freeze et al., 2012]. On interictal EEG at 8 days after birth, patient 1 revealed brief tonic seizures of the upper extremities and a diffuse spike or sharp and slow-wave complex, which were accompanied by brief suppression for 1–2 sec (Fig. 3I). At 50 days, she showed a series of spasms, and the EEG transited to hypsarrhythmia at 2 months, leading to a diagnosis of WS. The administration of adrenocorticotropic hormone (ACTH), zonisamide, and valproic acid (VPA) was temporarily effective; however, she developed seizures again at 4 months. Seizures were refractory to vitamin B6, phenobarbital, clobazam, corpus callosotomy, or a ketogenic diet. At 8 years of age, she showed hypotonia, severe intellectual disability, motor developmental delay, no head control, and no meaningful words. Patient 2 developed a series of spasms, and showed a diffuse spike or sharp and slow-wave complex on interictal EEG at 1 month. EEG transited to hypsarrhythmia at 4 months, leading to a diagnosis of WS. Her seizures were temporarily controlled by combined administration of VPA, nitrazepam, and ACTH, followed by low-dose ACTH therapy; however, spasms with clustering developed again at 6 years and 6 months. At 12 years, her spasms changed into focal seizures after administration of levetiracetam, and interictal EEG showed mainly slow waves with focal spikes. She could crawl on hands and knees and had severe intellectual disability with no meaningful words. Patient 3 started to have clusters of spasms at 3 months of age, and interictal EEG during sleep revealed hypsarrhythmia, leading to a diagnosis of early-onset WS (Fig. 3J). Vitamin B6 and VPA were ineffective at treating the spasms. Subsequent treatment with ACTH eliminated her spasms and hypsarrhythmia on EEG, but brief tonic seizures without clustering relapsed 1 month after the treatment. Despite the administration of various antiepileptic drugs

Table 1. Clinical Features of Patients with a *SLC35A2* Mutation

	Patient 1	Patient 2	Patient 3
Age	8 years 10 months	12 years 8 months	10 years 5 months
Gender	Female	Female	Female
Mutation	c.433_434del (p.Tyr145Profs*76)	c.972del (p.Phe324Leufs*25)	c.638C>T (p.Ser213Phe)
Diagnosis	EOEE → West syndrome	EOEE → West syndrome	Early-onset West syndrome
Initial symptom	Tonic seizure at 6 days	Spasms at 1 month	Spasms at 3 months
Initial EEG findings	Diffuse spike or sharp and slow-wave complex with brief suppression	Diffuse sharp or spike and slow-wave complex	Hypsarrhythmia
Transition of seizures	Spasms at 50 days, tonic seizure of upper extremities at 1 year 3 months	Generalized tonic seizure and spasm at 7 months, spasm at 6 years 6 months, focal seizure at 12 years	Brief tonic seizure, spasm at 1 year 6 months
Transition of EEG findings	Hypsarrhythmia at 2 months, multifocal spikes at 2 years	Hypsarrhythmia at 4 months, diffuse fast waves at 12 years	Multifocal spike and slow wave complex at 10 months
Seizure control	Intractable	Intractable	Intractable
Development	No head control, no words at 8 years	Crawling on hand and knees, no words at 12 years	No head control, no words at 10 years
Magnetic resonance imaging findings	Arachnoid pouch at 2 months, cerebral and cerebellar atrophy, thin corpus callosum, delayed myelination at 2 years	Normal at 2 months, spotty high-intensity signal in white matter, slight enlargement of left lateral ventricle at 4 years	Normal at 3 months, severe cortical atrophy, cerebellar atrophy, thin corpus callosum at 8 years
Craniofacial findings			
Coarse face	+	+	+
Thick eyebrows	+	+	+
Broad nasal bridge	+	+	+
Thick lips	+	+	+
Semi-open mouth	+	+	+
Prominent cupid's bow	–	+	+
Epicanthal folds	–	+	+
Short philtrum	–	+	+
Maxillary prognathism	+	+	+
Full cheek	–	–	+
Other	Fused tooth	High-arched palate	Enamel hypoplasia
Blood coagulation	Normal	Normal	Normal
Skin findings	Normal	Normal	Normal
Other features	Hypotonus	White spot in the eyeground, atrial septal defect ureteropelvic junction obstruction, vesicovaginal fistula	Hypotonic quadriplegia, hipdislocation

EOEE, early-onset epileptic encephalopathy; EEG, electroencephalography.

and a ketogenic diet, daily spasms with or without clustering have persisted. At the age of 10 years, she has attained no meaningful words or head control.

Discussion

In this study, we successfully identified three de novo heterozygous mutations in *SLC35A2* in patients with EOEE. Two mutations (p.Tyr145Profs*76 and p.Phe324Leufs*25) are predicted to cause truncation of UGT, suggesting that the function of the mutant protein would be severely impaired. Consistently, transient expression of mutant proteins in N2A cells revealed that the p.Phe324Leufs*25 mutant was not localized in the Golgi apparatus and that expression of the p.Tyr145Profs*76 mutant was severely diminished. Therefore, these two frameshift mutations are likely to cause loss of function in UGT. On the other hand, the p.Ser213Phe mutant was localized in the Golgi apparatus. A single amino acid deletion of Ser213 has been reported in hamster Ugt, which is highly homologous to human UGT (see Supp. Fig. S2). The hamster mutant failed to complement the defect of UDP-galactose transport in mutant Chinese hamster ovary lec8 cells, suggesting that the Ser213 residue is essential for proper UGT function [Oelmann et al., 2001]. Thus it is possible that the p.Ser213Phe mutation causes loss of function in the UGT, though further functional studies are required for clarifying pathogenicity of this missense allele.

Mutations in three nucleotide-sugar transporters have been previously reported to cause defects in glycan biosynthesis in humans: the GDP-fucose transporter encoded by *SLC35C1*, the CMP-sialic acid transporter encoded by *SLC35A1*, and the UDP-glucuronic acid/UDP-*N*-acetylgalactosamine transporter encoded by *SLC35D1* [Hiraoka et al., 2007; Liu et al., 2010; Lubke et al., 2001; Luhn et al., 2001; Martinez-Duncker et al., 2005]. Similarly, a defect in UGT would cause UDP-galactose deficiency in the ER–Golgi network, leading to reduced galactosylation of glycoproteins, glycosphingolipids, and proteoglycans [Liu et al., 2010]. In fact, three patients with *SLC35A2* mutations have been reported in association with galactosylation-deficient serum transferrin profiles in infancy: however, they showed normal serum transferrin profiles at 3–5 years [Ng et al., 2013]. Consistent with this, our three female cases showed no glycosylation abnormalities in the three commonly assayed serum glycoproteins at 8–10 years: transferrin and apolipoprotein CIII (mainly synthesized in the liver), and immunoglobulin G (synthesized by B lymphocytes) [Goreta et al., 2012; Okanishi et al., 2008; Wada et al., 2007, 2012]. In addition, DNA extracted from the leukocytes of patients 1 and 2 showed a markedly skewed X-inactivation, and only the WT *SLC35A2* allele was expressed in lymphoblastoid cell lines from these two patients. Therefore, although the degradation of mutant transcripts is a possible explanation for selective expression of WT allele, these findings raised a possibility that liver cells and B lymphocytes expressing the mutant allele are selected against during infancy, leading to no glycosylation defects in transferrin, apolipoprotein CIII, or immunoglobulin G in three patients, with a markedly skewed X-inactivation pattern in peripheral leukocytes.

The clinical features of the patients with a *SLC35A2* mutation seemed to be consistent with the negative selection of cells expressing the mutant allele. Specific skin features, coagulopathies,

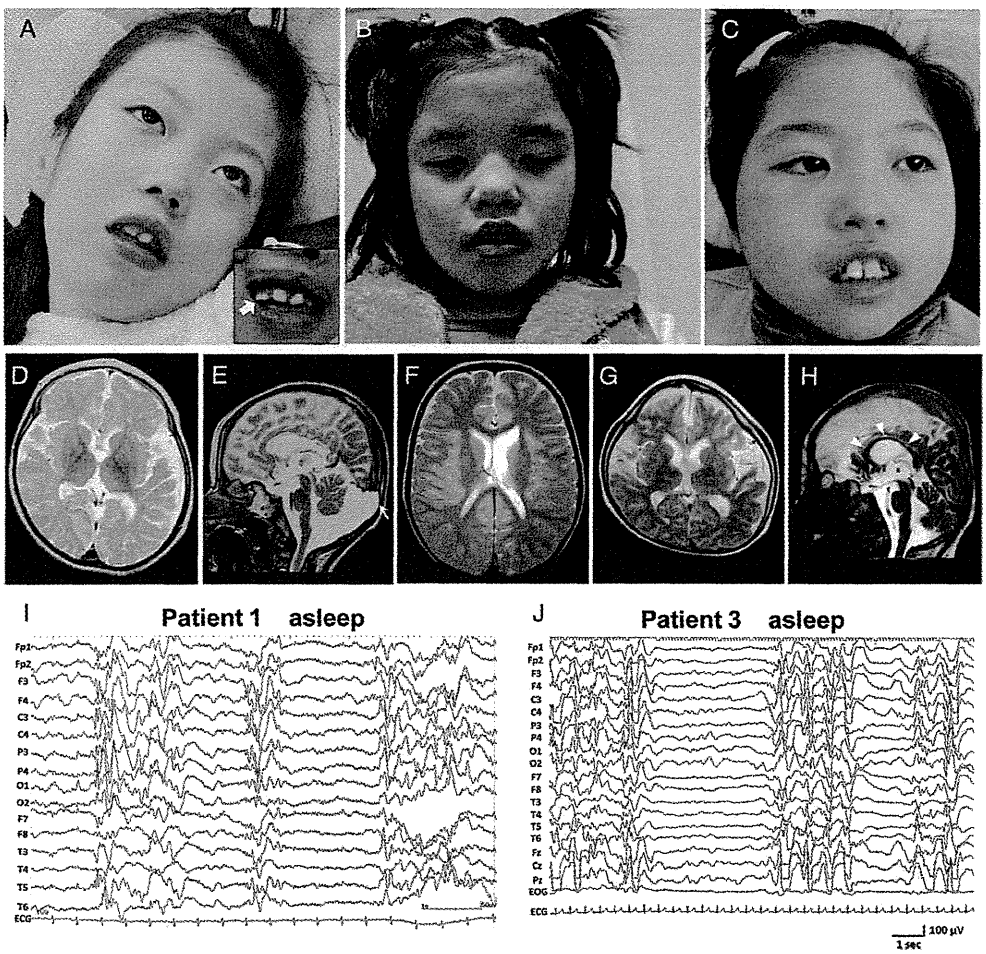

Figure 3. Facial appearance, brain (MRI), and EEG of the three patients with a *SLC35A2* mutation. **A–C**: Photograph of patient 1 at 8 years of age (**A**), patient 2 at 12 years of age (**B**), and patient 3 at 10 years of age (**C**). Note the broad nasal bridge, thick eyebrows, thick lips, semi-open mouth, and maxillary prognathism that are common in these three patients. A fused tooth observed in patient 1 is indicated by an arrow (**A**, inset). **D** and **E**: T2-weighted MRI of patient 1 at 2 years and 4 months after corpus callosotomy showed cerebral atrophy on an axial image (**D**), and cerebellar atrophy and an arachnoid pouch (white arrow) on a sagittal image (**E**). **F**: A T2-weighted axial image of patient 2 at 4 years and 3 months showed slight enlargement of the left lateral ventricle. **G** and **H**: T2-weighted MRI of patient 3 at 7 years showed cerebral atrophy with frontal lobe predominance on an axial image (**G**), and cerebellar atrophy and a thin corpus callosum (white arrowheads) on a sagittal image (**H**). **I**: Interictal EEG of patient 1 during sleep at 1.5 months old showing diffuse spike or sharp and slow-wave complexes, which were accompanied by brief suppression for 1–2 sec. **J**: Interictal EEG of patient 3 during sleep at 3 months old showing hypsarrhythmia.

immune dysfunction, cardiomyopathy, and renal dysfunction, which are often observed in glycosylation disorders [Freeze et al., 2012], were not found in these three patients, although they did present epileptic seizures (EOEE). Thus, it can be hypothesized that cells expressing the mutant allele were excluded in most organs but not the central nervous system, where a substantial number of neurons might express the mutant *SLC35A2* allele and suffer from defective galactosylation of glycoproteins, glycosphingolipids, and proteoglycans.

Together with a recent report [Ng et al., 2013], our data suggest that abnormal glycosylation may be one of the underlying pathologies of EOEE. In the absence of glycosylation abnormalities, similar to our three cases, a UGT disorder can only be diagnosed by the identification of a *SLC35A2* mutation. Recent progress in massively parallel DNA sequencing in combination with whole-exome capturing (WES) has facilitated rapid mutation detection in most exons [Bamshad et al., 2011]. WES is expected to be useful for genetic testing in EOEE, and is likely to reveal contributions from hitherto unexpected genes.

Conclusion

We identified de novo heterozygous mutations in the X-linked *SLC35A2* gene, which encodes the UGT, in patients with EOEE. Our data confirmed that abnormal glycosylation is one of the pathological features of EOEE.

Acknowledgments

The authors would like to thank all patients and their families for their participation in this study. We also thank Aya Narita and Nobuko Watanabe for technical assistance.

Disclosure statement: The authors declare no conflicts of interest.